Revised version 12-October-2012

Revisiting the "C-type adakites" in the Lower Yangtze River Belt, central eastern China: *in-situ* zircon Hf-O isotope and geochemical constraints

Xian-Hua Li[1]*, Zheng-Xiang Li[2], Wu-Xian Li[3], Xuan-Ce Wang[2], Yuya Gao[1]

1. State Key Laboratory of Lithospheric Evolution, Institute of Geology and Geophysics, Chinese Academy of Sciences, Beijing 100029, China

2. ARC Center of Excellence for Core to Crust Fluid Systems and The Institute for Geoscience Research, Department of Applied Geology, Curtin University, GPO Box U1987, Perth, WA 6845, Australia

3. State Key Laboratory of Isotope Geochemistry, Guangzhou Institute of Geochemistry, Chinese Academy of Sciences, Guangzhou 510640, China

Resubmitted to Chem Geol

*Corresponding author
E-mail: lixh@gig.ac.cn
Phone: 86-10-82998512
Fax: 86-10-62010846

Abstract

Adakites, or adakitic rocks in a broad sense, have been used to cover a large range of igneous rocks with a common feature of high Sr/Y and La/Yb ratios that can be achieved though different mechanisms. Amongst them, the continental, or C-type, adakitic rocks are particularly controversial in terms of their sources and genesis. In this study we revisit both Cu-Au ore-bearing and barren "C-type adakitic rocks" in the Lower Yangtze River Belt (LYRB) of central eastern China, including comprehensive analyses of their in-situ zircon Hf-O isotopes, whole-rock geochemistry and Sr-Nd isotopes. These "C-type adakitic rocks" consist of monzodiorite, granodiorite and quartz monzonite that are classified as shoshonitic to high-K calc-alkaline series in terms of their chemical compositions. They are characteristically high in potassium (K_2O = 2.4–4.5%, K_2O/Na_2O = 0.6–1.3), with continental crust-like isotopic compositions, i.e., whole-rock εNd(T) = -3.9 to -7.7, initial $^{87}Sr/^{86}Sr$ = 0.7054–0.7085, zircon εHf(T) = 0 to -11, and $\delta^{18}O$ = 6‰ to 9‰. The ore-bearing and barren rocks are cogenetic. Fractional crystallization of hornblende, titanite, magnetite and apatite plays a major role in their chemical variations, with the ore-bearing rocks being more felsic (SiO_2 = 63.3–69.6%) and higher in Sr/Y (41.2–75.6) than the barren rocks (SiO_2 = 57.3–65.0%, Sr/Y =30.4–51.8). All these geochemical and isotopic features, in combination with regional geological data, suggest that the LYRB "C-type adakitic rocks" were unlikely to have been formed by melting of either a thickened and/or delaminated lower continental crust, or an altered oceanic crust as previously thought. These rocks are in general akin in geochemistry and isotopes to the Archean

sanukitoids and the Setouchi high-Mg andesites in Japan, and are thus interpreted as being formed by melting of an enriched mantle source metasomatized by dewatering from a delaminated flat-slab. The flat subduction of an oceanic plateau and its subsequent delamination and foundering since early Mesozoic beneath southeastern China (Li and Li, 2007) thus not only explain the temporal and spatial propagation of widespread Yanshanian igneous rocks regionally since ca. 195 Ma, but also the formation of a series of enigmatic "adakitic" rocks in the region, including the LYRB potassium-rich rocks that were inappropriately called the "C-type adakitic rock" by previous workers.

Keywords: adakites; granites; mineralization; zircon Hf-O isotopes; Yangtze River; China

1 Introduction

The term "adakite" was first coined by Defant and Drummond (1990) to describe a group of intermediate to felsic volcanic or intrusive rocks in Cenozoic arcs associated with subduction of young (<25 Ma) oceanic lithosphere. These rocks have salient geochemical and isotopic features (e.g., sodic, aluminous, strongly depleted in HREE and Y, high in Sr/Y and La/Yb and MORB-like Sr and Nd isotopes) believed to be the results of partial melting of the basaltic portion of oceanic crust subducted beneath volcanic arcs. Adakite genesis and their implications for tectonic environments and porphyry copper mineralization have gained wide interests in the past two decades, and the term of “adakite” has been increasingly used for a much wider range of rock types than originally defined. In addition to slab melting, adakites, and/or adakitic rocks with similar geochemical features to the oceanic slab-derived adakites, are now believed to have been generated by other petrogenetic processes as well, such as (1) partial melting of thickened mafic lower crust triggered by underplating of hot basaltic magmas, (2) melting of delaminated lower crust in the mantle, (3) high-pressure fractionation of garnet and amphibole from hydrous basaltic magma, and (4) crustal assimilation and fractional crystallization of basaltic magmas (e.g., Castillo, 2006, 2012 and references therein). Among the numerous adakites and/or adakitic rocks that have been investigated, the “continental” (also named “C-type” or “potassic”) adakitic rocks, i.e., rocks formed through genesis 1 and 2 above (e.g., Zhang et al., 2001; Rapp et al., 2002; Xu et al., 2002; Wang et al., 2004a; Xiao and Clemens, 2007), have caused some confusions and debates. Despite being

geochemically similar to the modern slab-derived adakites, most “C-type” adakitic rocks are potassium-rich and isotopically akin to the continental crust.

The Lower Yangtze River Belt (LYRB) in central eastern China is one of the type localities where the “C-type” adakitic rocks were first proposed (e.g., Zhang et al., 2001; Xu et al., 2002). Because the LYRB “C-type” adakitic rocks are closely associated with Cu-Au mineralization, their genesis has attracted wide attention in the past decades. Models for their generation usually invoke partial melting of thickened and/or delaminated lower continental crust (e.g., Zhang et al., 2001; Xu et al., 2002; Wang et al., 2004a, b, 2006a, 2007). Alternatively, some other workers suggested, on the basis of geochemical and isotopic investigations, that the LYRB ore-bearing adakitic rocks represent partial melts of altered oceanic crust associated with assimilation of enriched components in the lithospheric mantle and/or crustal materials (Liu et al., 2010; Ling et al., 2009, 2011; Sun et al., 2010). To clarify the genesis of the LYRB “C-type” adakitic rocks, we carried out an integrated *in-situ* zircon Hf-O isotope, bulk-rock geochemistry and Sr-Nd isotope study on both ore-bearing and barren “C-type” adakitic rocks in the Edong and Jiurui mining districts of the western LYRB. The aims of our work include: (1) understanding the genetic relationship between the LYRB ore-bearing and barren “C-type” adakitic rocks, (2) providing further constraints on the source of these LYRB adakitic rocks by comparing these “C-type” adakitic rocks with other high Sr/Y rocks, and (3) exploring regional petrotectonic implications.

2 Geological background

The eastern part of the Yangtze Craton is separated by the Dabie-Sulu Orogen from the North China Craton in the north, and by the Jiang-Shao Fault from the Cathaysia Block in the south (Fig. 1A). The basement rocks of the Yangtze Craton are exposed in the Kongling area near the Yangtze Gorge Dam, consisting of the Archean to Paleoproterozoic high-grade metamorphic TTG (tonalite, trondhjemite and granodiorite) gneisses, metasedimentary rocks and amphibolites (e.g., Gao et al., 1999, 2011; Jiao et al., 2009). The LYRB is situated along the Yangtze River Valley in the northeastern part of the Yangtze Block (Fig. 1B). There are no pre-Neoproterozoic rocks exposed in the LYRB; stratigraphic units in this area include late Neoproterozoic low-grade metasedimentary rocks and intercalated metavolcanic rocks, latest Neoproterozoic to Middle Triassic marine clastic sedimentary rocks and carbonates, Upper Triassic to Jurassic lacustrine and swamp-facies sedimentary rocks and intercalated coal beds, and Cretaceous evaporates, red beds and terrestrial volcanic rocks. Magmatic rocks dated at ca. 146–120 Ma (e.g., Mao et al., 2006; Zhou et al., 2008; J.W. Li et al., 2009; X.H. Li et al., 2010a) are concentrated in seven mining districts along the LYRB, including more than 260 intrusions with individual outcrop areas >0.2 km^2 (e.g., Chang et al., 1991; Zhai et al., 1992). Ore mineralization associated with the igneous rocks can be grouped into two major series: (1) relatively Si-rich, high-K calc-alkaline rock series related to Cu-Au-Mo-Pb-Zn-(Fe) polymetallic mineralization, and (2) relatively Si-poor, high-Na calc-alkaline rock series related to the “Daye-type” Fe (Cu, Co, S) and “Ningwu-type” Fe (S, V, Ti, P)

mineralization (Chang et al., 1991). Granodioritic porphyries with adakite-like geochemistry are the most important intrusions associated with the first series of Cu-Au-(Mo) polymetallic mineralization (e.g., Wang et al., 2001, 2004a, b, c, 2006a, 2007; J.W. Li, et al., 2008, 2009; Ling et al., 2009).

The Jiurui and Edong mining districts are located at the western part of the LYRB (Fig. 1B). In the Jiurui district, numerous small porphyries intruded the Paleozoic to Lower Triassic clastic sedimentary rocks and carbonates (Fig. 1C). Among them, granodiortic porphyries at the Chengmenshan, Wushan and Fengshan areas host important porphyry-skarn type Cu-Au-(Mo) polymetallic mineralization (e.g., Pan and Dong, 1999). These rocks display porphyritic texture; phenocrysts are mainly plagioclase and quartz as well as subordinate hornblende and biotite, with a typical grain size of 0.8–2 mm. The matrix shows a fine-microcrystalline texture, consisting of quartz, K-feldspar, plagioclase, hornblende and biotite. Accessory minerals include magnetite, apatite, zircon and titanite. Molybdenite Re-Os and zircon U-Pb isotopic dating results indicate that these porphyries and associated mineralization formed synchronously at ca. 146–144 Ma (Xie et al., 2006a; J. Li et al., 2007; X.H. Li, 2010a).

In the Edong district, several major intrusions associated with two series of mineralization were emplaced into the Paleozoic to Lower Triassic clastic sedimentary rocks and carbonates. The “Daye-type” skarn Fe (Cu, Co, S) mineralization is associated with the Echeng, Tieshan and Jinshandian plutons dated at ca. 136–120 Ma (J.W. Li et al., 2009) in the northern Edong district. The

porphyry-skarn type Cu-Au polymetallic mineralization at the Tonglushan and Tongshankou mines is associated with the Yangxin and Lingxiang plutons, respectively, in the southern Edong district (Fig. 1D). The Yangxin and Lingxiang plutons are composed of predominant medium-grained diorite and subordinate quartz diorite and granodiorite. The Tonglushan and Tongshankou granodioritic porphyries show porphyritic textures. Phenocrysts are mainly plagioclase and biotite, with a typical grain size of 0.5–1.5 mm. The matrix consists of plagioclase, K-feldspar, quartz, hornblende and biotite as well as accessory minerals including magnetite, titanite, zircon and apatite. The Yangxin pluton and the associated Tonglushan Cu-Au-(Fe) mineralized porphyry were dated at ca. 140 Ma, whilst the Liangxiang pluton and the associated Tongshankou Cu-Mo mineralised porphyry were dated at ca. 145 Ma (X.H. Li et al., 2010).

The Yinzu pluton, located in the southernmost Edong district (Fig. 1D), is the sole intrusion that is not related to any mineralization in the Edong mining district. Medium-grained granodiorite dominates the pluton. Rock-forming minerals include plagioclase, K-feldspar, quartz, biotite and hornblende; the accessory minerals include magnetite, titanite, zircon, and apatite. It was dated at ca. 146 Ma (X.H. Li et al., 2010), synchronous with the adjacent Liangxiang pluton and Tongshankou porphyry.

In-situ zircon Hf-O isotopes and whole-rock geochemistry and Sr-Nd isotopes were analyzed in this study for the previously-recognized “C-type” adakitic rocks. These rocks include the Cu-Au-(Mo) ore-bearing porphyries (Chengmenshan, Wushan, Dongleiwan and Dengjiashan in the Jiurui district and Tonglushan and

178 Tongshankou in the Edong district) and their coeval ore-barren plutons (Yangxin,
179 Lingxiang and Yinzu in the Edong district).
180
181 **3 Analytical methods**
182 **3.1 SIMS zircon oxygen isotopes**
183 Oxygen isotope measurements were conducted on the zircons previously used for
184 SIMS U-Pb dating (X.H. Li et al., 2010a). After U-Pb dating, the sample mount was
185 re-ground and re-polished to ensure that any oxygen implanted in the zircon surface
186 from the O_2^- beam used for U-Pb analysis was removed. Zircon oxygen isotopes were
187 measured using the Cameca IMS-1280 SIMS at the Institute of Geology and
188 Geophysics, Chinese Academy of Sciences (IGG-CAS) in Beijing, with analytical
189 procedures similar to those reported by X.H. Li et al. (2010b)**.** The Cs^+ primary ion
190 beam was accelerated at 10 kV, with an intensity of ca. 2 nA corresponding to a beam
191 size of 10 μm in diameter. A normal incidence electron flood gun was used to
192 compensate for sample charging. Negative secondary ions were extracted with a -10
193 kV potential. Oxygen isotopes were measured using the multi-collection mode.
194 Uncertainties on individual analyses are reported at 1σ level. The internal precision of
195 a single analysis is generally better than 0.2‰ (2σ standard error) for $^{18}O/^{16}O$ ratio.
196 The instrumental mass fractionation factor (IMF) is corrected using the 91500
197 zircon standard with $\delta^{18}O_{VSMOW}$ = 9.9‰ (Wiedenbeck et al., 2004). Measured $^{18}O/^{16}O$
198 is normalized using the Vienna Standard Mean Ocean Water compositions (VSMOW,
199 $^{18}O/^{16}O$ = 0.0020052), and reported in standard per mil notation. The instrumental

mass fractionation factor (IMF) is corrected as follows:

$$(\delta^{18}O)_M = (\frac{(^{18}O/^{16}O)_M}{0.0020052} - 1) \times 1000 \quad (‰)$$

$$IMF = (\delta^{18}O)_{M(standard)} - (\delta^{18}O)_{VSMOW}$$

$$\delta^{18}O_{Sample} = (\delta^{18}O)_M - IMF$$

During the course of this study, Temora 2 zircon standard was also measured as an unknown to monitor the external precision. Forty measurements of Temora 2 yielded a weighted mean $\delta^{18}O$ = 8.18 ± 0.36‰ (2σ standard deviation), which is consistent within errors with the reported value of 8.20‰ (Black et al., 2004). SIMS oxygen isotopic data are listed in Appendix Table 1.

3.2 LA-MC-ICPMS Hf isotopes

In-situ zircon Lu-Hf isotopic analysis was carried out on a Neptune MC-ICPMS equipped with a Geolas-193 laser-ablation system at the IGG-CAS. Lu-Hf isotopic analyses were obtained on the same zircon grains that were previously analyzed for U-Pb and O isotopes, with ablation pits of 63 μm in diameter, ablation time of 26 seconds, repetition rate of 10 Hz, and laser beam energy density of 10 J/cm^2. The detailed analytical procedures were similar to those described by Wu et al. (2006). The isobaric interference of ^{176}Lu on ^{176}Hf was corrected by measuring the intensity of the interference-free ^{175}Lu isotope and using a recommended ^{176}Lu/^{175}Lu ratio of 0.02655 (Machado and Simonetti, 2001). The isobaric interference of ^{176}Lu on ^{176}Hf is minor since the measured ^{176}Lu/^{177}Hf for unknowns are normally lower than 0.003 in this study. On the other hand, the interference of ^{176}Yb on ^{176}Hf must be carefully

corrected since the contribution of ^{176}Yb to ^{176}Hf could affect the accuracy of the measured $^{176}Hf/^{177}Hf$ ratio. The mean $^{173}Yb/^{172}Yb$ ratio of the individual spots was used to calculate the fractionation coefficient (β_{Yb}) and the contribution of ^{176}Yb to ^{176}Hf by applying ratios of $^{176}Yb/^{172}Yb = 0.5887$ and $^{173}Yb/^{172}Yb = 0.73925$ (Wu et al., 2006, 2010). The measured $^{176}Yb/^{177}Hf$ ratios, apart from a few analyses from samples 08YZ9.1 and 08YZ14.5, are between 0.01-0.03 for unknowns in this study. They are generally lower than the $^{176}Yb/^{177}Hf$ ratio of ~0.03 for Temora 2 standard zircon, thus have little effect on the accuracy of the $^{176}Hf/^{177}Hf$ ratios (Wu et al., 2006). Measured $^{176}Hf/^{177}Hf$ ratios were normalized to $^{179}Hf/^{177}Hf = 0.7325$. No further external adjustments were applied for the unknowns because our determined $^{176}Hf/^{177}Hf$ ratios for 91500 zircon (0.282302 ± 0.000020, 2σ standard deviation) and Temora 2 zircon (0.282676 ± 0.000018, 2σ standard deviation) were in good agreement with the reported values (e.g. Goolaerts et al., 2004; Wu et al., 2006; Blichert-Toft, 2008). Initial εHf(T) values are calculated by using the U-Pb ages with the reference to the chondritic reservoir (CHUR) at the time of zircon crystallization from magmas. Because of extremely low $^{176}Lu/^{177}Hf$ ratios, the difference between the measured and the age-corrected initial $^{176}Hf/^{177}Hf$ ratios is mostly between 0.000002 and 0.000005 for the unknowns. Zircon Lu-Hf isotopic data are also listed in Appendix Table 1.

3.3 Major and trace elements

After petrographic examinations, the least-altered whole-rock samples, except for

3 samples from the Chengmenshan and Wushan Mines that show strong potassium alteration, were selected for geochemical and Sr-Nd isotopic analyses. Major-element oxides were analyzed using a Rigaku RIX 2000 X-ray fluorescence spectrometer at the Guangzhou Institute of Geochemistry (CAS) on fused glass beads. Calibration lines used in quantification were produced by bivariate regression of data from 36 reference materials encompassing a wide range of silicate compositions (X.H. Li et al., 2005), and analytical uncertainties are between 1% and 5%. Trace elements were analyzed using a Perkin-Elmer Sciex ELAN 6000 ICP-MS at the Guangzhou Institute of Geochemistry (CAS). Analytical procedures are similar to those described by X.H. Li et al. (2000). About 50 mg of each powdered sample was dissolved in a high-pressure Teflon bomb for 24 hr using a HF + HNO_3 mixture. An internal standard solution containing the single element Rh was used to monitor signal drift during counting. A set of USGS and Chinese national rock standards were chosen for calibration, and analytical precision is typically <5%. Major and trace element data are listed in Appendix Table 2.

3.4 Sr and Nd isotopes

Whole-rock powders for Sr and Nd isotopic analyses were dissolved using mixed HF+HNO_3 acid in Teflon bombs at ca. 200 ℃ for two days. Sr and rare earth elements (REEs) were separated using the columns filled with 2 mL of AG50W×12 cation-exchange resin. The detailed chemistry procedures for separation of Sr and REEs from the sample matrix are as same as those reported by C.F. Li et al. (2012).

Nd fractions were further separated by bis(2-ethylhexyl) hydrogen phosphate (HDEHP)-coated teflon columns. Strontium and Nd isotopic ratios were measured using a Finnigan MAT262 multi-collector mass spectrometer at the IGG-CAS. Detailed analytical procedures are similar to those described by Yang et al. (2004). The whole procedure blank for Nd and Sr is lower than 0.07 ng and 0.2 ng, respectively. Measured $^{87}Sr/^{86}Sr$ and $^{143}Nd/^{144}Nd$ ratios were normalized to $^{86}Sr/^{88}Sr$ = 0.1194 and $^{146}Nd/^{144}Nd$ = 0.7219, respectively. The measured values for the NBS987 Sr standard and JNdi-1 Nd standard were $^{87}Sr/^{86}Sr$ = 0.710253 ± 20 (2σ standard deviation, n = 5) and $^{143}Nd/^{144}Nd$ = 0.512115 ± 12 (2σ standard deviation, n = 5), respectively. The USGS reference material BCR-2 was measured as an unknown to monitor the accuracy of the analytical procedures. Three measurements yielded $^{87}Sr/^{86}Sr$ = 0.704989 ± 20 (2σ standard deviation, n = 3) and $^{143}Nd/^{144}Nd$ = 0.512629 ± 14 (2σ standard deviation, n = 3), indistinguishable within reported errors with the recommended values (Raczek et al., 2003). Sr and Nd isotopic data are listed in Appendix Table 3.

4 Results

4.1 Whole-rock geochemistry

Twenty-eight ore-bearing and eighteen barren rock samples were analyzed for major and trace elements. Apart from three ore-bearing samples (08YZ9.1, 08YZ9.2 and 08YZ12.6) that are strongly altered as shown by high LOI value of 4.0-6.4% and exceptionally low Na_2O content of ~0.2% (Appendix Table 2), the remaining 43

288 samples are relatively fresh (LOI value mostly <2%), and their geochemical
289 compositions are used for discussions below. The ore-barren samples have relatively
290 low SiO_2 content between 57.3% and 65.0%. With increasing SiO_2, TiO_2, MgO,
291 $Fe_2O_3^T$, CaO, P_2O_5, MnO, Sc and Y decrease, and Al_2O_3 (16-17%) and Na_2O
292 (3.5-4.3%) remain roughly constant (Fig. 2). On the TAS (K_2O + Na_2O *vs.* SiO_2)
293 diagram (Fig. 3), samples with SiO_2 ≤61% plot in the monzodiorite filed of the
294 shoshonitic series, whilst the remaining samples with SiO_2 of 63-65% plot in the
295 granodiorite and quartz monzonite field of the high-K calc-alkaline series.

296 The ore-bearing samples have relatively high SiO_2 content (63.3-69.6%) and
297 follow the same geochemical trends as the barren samples (Fig. 2), but with slightly
298 higher K_2O (2.6-4.5%) and lower Al_2O_3 (14-17%). Most of them plot in granodiorite
299 and quartz monzonite field of the high-K calc-alkaline series. The highly coherent
300 behaviors in major and trace elements (Fig. 2, 3) indicate that the ore-bearing and
301 barren rocks are likely cogenetic.

302 The ore-barren rocks show similar Chondrite-normalized REE patterns, with
303 variable LREE enrichment (La_N = 113-220, Yb_N = 7.3-11.7 and La_N/Yb_N = 12.1-23.1,
304 subscript N denotes the Chondrite-normalized) and insignificant Eu anomaly (Eu/Eu*
305 = 0.81-0.99) (Fig. 4A). Thus, crystal fractionation of feldspars must have played an
306 insignificant role in the magmatic evolution, consistent with the roughly constant
307 Al_2O_3 contents (Fig. 2). In the primitive mantle-normalized incompatible trace
308 element spidergrams (Fig. 4B), these rocks show strong positive Pb anomaly and
309 variable enrichment in Rb, Ba, Th, U, Pb, Sr and LREE and depletion in Nb, Ta, P,

and Ti. Similarly, the ore-bearing rocks also display LREE-enriched patterns without obvious Eu anomaly (Eu/Eu* = 0.82-1.02) (Fig. 4C). Compared with the barren rocks, the ore-bearing rocks have slightly higher abundances in LREE (La_N = 121-298) and lower in HREE (Yb_N = 5.3-10.4), consequently they display more fractionated LREE/HREE (La_N/Yb_N = 16.7-49.7). In the primitive mantle-normalized spidergrams, the ore-bearing rocks display similar trace element patterns to the barren rocks, with relatively low abundances in HREE (Fig. 4D). On the Sr/Y *vs.* Y and La *vs.* $(La/Yb)_N$ diagram (Fig. 5), the ore-barren rocks straddle the overlapping field of adakite and "normal" andesite-dacite-rhyolite, whereas the ore-bearing rocks have relatively higher Sr/Y and lower Y than the barren ones, mostly plotting in the adakite field.

4.2 In-situ zircon O and Hf isotopes

One hundred and eleven *in-situ* O and Hf isotope analyses were conducted on 111 zircons from the ca. 145 Ma ore-bearing rocks (including the Tongshankou, Chengmenshan, Wushan, Dongleiwan and Dengjiashan porphyries), and 38 analyses on 38 zircons from the ore-barren rocks (including the Liangxiang and Yinzu plutons. All these zircons crystallized at ca 145 Ma (X.H. Li et al., 2010), and most of them are euhedral, transparent, and 100-300 μm in length with aspect ratios between 2:1 and 3:1. They are all characterized by euhedral concentric zoning in cathodoluminescence (CL) images (Fig. 6). For the ore-bearing rocks, the measured zircon $^{176}Hf/^{177}Hf$ ratios range from 0.282343 to 0.282705, corresponding to the εHf(T) values from −12.1 to 0.5; the measured $\delta^{18}O$ values are between 6.4‰ and

9.2‰ (Fig. 7A and B, Appendix Table 1). Zircons from the ore-barren rocks have $^{176}Hf/^{177}Hf$ ratios ranging from 0.282414 to 0.282695, corresponding to the εHf(T) values from –9.5 to 0.4, and $\delta^{18}O$ values from 6.6‰ to 8.2‰ (Fig. 7A and B, Appendix Table 1). Overall, zircons from the ca. 145 Ma ore-bearing and barren rocks have similar ranges of Hf and O isotopes, apart from a few grains from the ore-bearing rocks that have εHf(T) value lower than –10 and $\delta^{18}O$ value higher than 8.5‰. There is no obvious correlation between εHf(T) and $\delta^{18}O$ values (Fig. 7C).

Eighteen and 39 *in-situ* zircon O and Hf isotopes were conducted on one ca. 140 Ma Tonglushan ore-bearing porphyry (08YZ33.4) and two ore-barren rocks (08YZ15.1 and 08YZ16.5) from the Yangxin pluton, respectively. The Tonglushan zircons have $^{176}Hf/^{177}Hf$ ratios ranging from 0.282387 to 0.282544, corresponding to the εHf(T) values from –10.6 to –5.0, and $\delta^{18}O$ values from 6.0‰ to 8.6‰ (Fig. 7D and E, Appendix Table 1). The Yangxin zircons have relatively high $^{176}Hf/^{177}Hf$ ratios, ranging from 0.282460 to 0.282571, corresponding to the εHf(T) values from -8.9 to 0.4, and low $\delta^{18}O$ values of between 5.8 ‰ and 7.8‰ (Fig. 7D and E, Appendix Table 1). The combined dataset form a weak, negative correlation between εHf(T) and $\delta^{18}O$ values (Fig. 7F).

4.3 Whole-rock Sr-Nd isotopes

Seventeen ore-bearing and 11 barren rock samples were analyzed for Sr and Nd isotopes. Apart from 3 altered ore-bearing rocks (08YZ9.1, 08YZ9.2 and 08YZ12.6), the remaining samples have a limited range of Sr and Nd isotopic compositions (Fig.

354 8), with the initial $^{87}Sr/^{86}Sr$ ratio (I_{Sr}) = 0.7054 to 0.7085 and εNd(T) = –3.9 to –7.7
355 (Appendix Table 3). Three altered ore-bearing rocks exhibit comparable εNd(T)
356 values with the least-altered rocks, but much higher I_{Sr} values of 0.7118 to 0.7160,
357 indicating that alteration processes significantly influenced the Rb-Sr isotopic system,
358 but had little, if any, effect on the Sm-Nd system of these rocks.
359
360 **5 Discussions**
361 While the LYRB ore-bearing adakitic rocks have been widely investigated, less
362 attention has been paid to the genesis of the associated barren rocks, and the
363 relationship between the ore-bearing and barren rocks is also an issue of debate. Wang
364 et al. (2004b, c) proposed that the ore-bearing adakitic porphyries at Tongshankou
365 originated from partial melting of delaminated lower crust with garnet being the main
366 residual mineral, whereas the nearby Yinzu barren rocks resulted from partial melting
367 of thickened lower crust with residual garnet ± plagioclase ± hornblende. Contrarily,
368 J.W. Li et al. (2009) interpreted that the Yinzu rocks were generated by low-pressure
369 fractional crystallization of mantle-derived mafic magmas in response to the late
370 Mesozoic lithospheric extension and thinning in eastern China.
371 The barren rocks are not only closely associated in time and space with the
372 ore-bearing porphyries, but also volumetrically dominant. Therefore, integrated and
373 comparative investigations of whole-rock geochemistry and Sr-Nd isotopes, and
374 in-situ zircon Hf-O isotopes for these barren and rocks, will not only provide robust
375 constrain on their genesis, but also shed new light on the sources of the coeval

ore-bearing adakitic porphyries.

5.1 Magmatic processes

Major and trace element data for the studied ore-bearing and barren rocks show coherent trends (Fig. 2 and 3), with the barren rocks being relatively more mafic (SiO_2 = 57.3-65.0%) than the ore-bearing porphyries (SiO_2 = 63.3-69.6%). Such geochemical variations could be attributed to different magmatic processes such as fractional crystallization of common parental magmas, partial meting of mafic igneous sources, and magma mixing. Because of their limited Sr and Nd isotopic variations and the lack of any correlation between Sr-Nd isotopes and SiO_2 (not shown), magma mixing and/or assimilation of crustal materials, as indicated by the existence of a few old xenocrystal zircons (X.H. Li et al., 2010), were unlikely the dominant mechanisms for the chemical variations of the studied rocks. Figure 9 is a log-log diagram (Cocherie, 1986) of correlation between compatible and incompatible trace elements, which has been demonstrated to be an effective way of distinguishing fractional crystallization from partial melting. It shows that Sc decreases rapidly with a relatively small increase in Rb, suggesting that fractional crystallization played a major role in the chemical variations of the studied rocks. Decreases in MgO, Fe_2O_3, CaO, TiO_2, P_2O_5 and Sc with increasing SiO_2 (Fig. 2) indicate fractional crystallization of hornblende, titanite, magnetite and apatite. The lack of obvious Eu negative anomaly (Fig. 4A and C) and nearly constant Al_2O_3 over a wide range of SiO_2 content (Fig. 2) suggest insignificant fractional crystallization of feldspars.

Therefore, the parental magmas of the studied rocks should be more mafic than the least-evolved Yangxin monzodiorite sample 08YZ16.5 (SiO_2 = 57.3%). If this deduction is correct, the parental magmas should be potassium-rich basalt to basaltic andesite in compositions.

We performed a modeled Rayleigh fractionation of hornblende, titanite and magnetite from an andesite melt (SiO_2 = 57%, Sr = 690 ppm, Y = 23 ppm, Sc = 25 ppm, Yb = 2.5 ppm, La = 36 ppm, Rb = 80 ppm). Because REE, high field strength elements (HFSE) and transition element (Sc) are highly compatible into titanite and hornblende (Bachmann et al., 2005; Klein et al., 1997; LaTourrette et al., 1995; Prowatke and Klemme, 2005; Richards and Kerrich, 2007; Sisson, 1994), their partition coefficients are important parameters for geochemical modeling of petrogenetic processes. Experimental studies have demonstrated that melt compositions strongly affect the partitioning of trace elements between titanite and silicate melt (Prowatke and Klemme, 2005). Compilation of experiment determined hornblende-melt partition coefficient dataset (LaTourrette et al., 1995; Richards and Kerrich, 2007; Sisson, 1994) indicates that melt silicate contents also affect the partition coefficients of Sc, Yb and Y between hornblende and melts. These three elements behave moderately incompatible to slightly compatible in hornblende at basalt-basaltic andesite system (SiO_2<57 wt.%). By contrast, with increasing silica content, Sc, Yb and Y are highly compatible into hornblende. Therefore, geochemical modeling of petrogenetic processes must consider the effect of melt compositions on the melt-mineral partition coefficients. As a consequent, a two-stage modeled

Rayleigh fractionation is applied to constrain the effect of hornblende associated with titanite and magnetite. The modeling results are plotted in Figs. 5 and 10, and the partition coefficients from Sisson (1994) and Prowatke and Klemme (2005) are listed in Appendix Table 5.

The first-stage involves fractionation of 10% hornblende and 5% magnetite. Experimental data showed that hornblende crystallized from basaltic to andesitic samples possess SiO_2 = 40-44% and $Fe_2O_3^T$ = 7-12 wt.% (Klein et al., 1997; LaTourrette et al., 1995; Sisson, 1994). As shown in Fig. 2, decreasing SiO_2 from 57% to 65% corresponds to ~4 wt.% depletion of $Fe_2O_3^T$. This requires ~5% magnetite fractional crystallization if $Fe_2O_3^T$ is 70% and 20% in magnetite and hornblende, respectively. When the magma evolved from an andesitic melt with SiO_2 = 57% (the lowest silicate sample in this study), mass-balance suggests fractional crystallization of 10% hornblende associated with 5% of magnetite would result in a residual melt with ~64 wt.% SiO_2 and ~4 wt.% $Fe_2O_3^T$. Because La, Yb, Y, Sr and Rb are highly incompatible in magnetite in all melts, Sc is incompatible in magnetite within basalt-andesite melt, but only slightly compatible within high-silica melt, the effect of magnetite fractionation on La, Yb, Y, Sr, Rb and Sc is ignored.

The second-stage involves fractionation of 7.2% hornblende, 0.1% titanite and 2.7% magnetite (proportions relative to the original magma system) from the residual melt (SiO_2 = 64%). Because Yb, Y and Sc behave highly compatible in siliceous melt, the modeling shows that ~10% fractionation of hornblende, titanite and magnetite at the second-stage will significantly deplete Yb, Y and Sc. This modeling results match

well with the observed geochemical trends (Figs. 5 and 9), indicating that fractional crystallization of ~17.2% hornblende, ~0.1% titanite and ~5.7% magnetite from an andesitic melt (SiO_2 = 57%) could account for the adakite-like Sr/Y and La/Yb ratios for the LYRB ore-bearing rocks.

5.2 Magma sources

The magma sources for the LYRB "adakitic rocks" are highly controversial. Many previous workers invoked thickened and/or delaminated lower continental crust as the sources for these rocks (Zhang et al., 2001; Xu et al., 2002; Rapp et al., 2002; Wang et al., 2004a, b, c, 2006a, 2007). More recently, it has been proposed that the LYRB "adakitic rocks" were generated by partial melting of altered oceanic crust, possibly in a slab window created by a subducted mid-ocean ridge (Ling et al., 2009, 2011; Liu et al., 2010; Sun et al., 2010). J.W. Li (2009) further speculated that some of these rocks from the Edong mining district were derived from an enriched lithospheric mantle.

5.2.1 Melting of thickened continental crustal model

In comparison with typical slab-derived adakites that are characteristically sodium-rich (Na_2O >3.5%, $K_2O/Na_2O \approx 0.4$) with MORB-like isotopic compositions (such as $^{87}Sr/^{86}Sr$ <0.7045) (see compilation of Richards and Kerrich, 2007), the LYRB "adakitic rocks" are potassium-rich (Fig. 10 for results of this study, where K_2O/Na_2O = 0.6-1.3) with continental crust-like isotopic compositions (I_{Sr} = 0.7054 to

464 0.7085 and εNd(T) = –4.3 to –7.7). Such distinct geochemical and isotopic features
465 prompted some researchers (e.g., Zhang et al., 2001; Xu et al., 2002; Wang et al.,
466 2004a, b, c, 2006a, 2007) to propose that the LYRB "adakitic rocks" were formed by
467 partial melting of a thickened or delaminated lower continental crust ("C-type"
468 adakites). Wang et al. (2004b, c) further proposed two groups of "C-type" adakites for
469 the ore-bearing and barren intrusions in the Edong district. One group is typified by
470 the Cu-bearing Tongshankou porphyry that is characterized by relatively high SiO_2
471 and Sr/Y but low $Fe_2O_3^T$; it was interpreted to be formed by melting of delaminated
472 lower continental crust materials in the lithospheric mantle. Another group is typified
473 by the Yinzu barren pluton that is relatively low in SiO_2 and Sr/Y but high in $Fe_2O_3^T$,
474 which is thought to be formed by melting of a thickened lower continental crust. Such
475 a petrogenic interpretation requires the existence of a thickened lower continental
476 crust (LCC) prior to the formation of these rocks.

477 However, the required LCC thickening is inconsistent with the regional basin
478 history, i.e. changing from a foreland basin south of the Dabie Orogen in early
479 Mesozoic (Grimmer et al., 2003) to extensional basins in late Mesozoic (Ling et al.,
480 2009). There is also no evidence for regional crustal uplifting responding to the
481 delamination of a thickened lower crust. The Nd isotopic compositions of the studied
482 adakitic rocks are also inconsistent with such a model. The LCC basement rocks for
483 the Yangtze craton, represented by the Archean Kongling Group rocks (Gao et al.,
484 1999) and the LCC-derived granitoid rocks from the Dabie Orogen and northeastern
485 Yangtze Block (Liu et al., 2010 and references therein), have significantly lower Nd

isotopic compositions than the studied LYRB adakitic rocks (Fig. 8). The LYRB "adakitic" rocks have a restricted Th/U ratio of 3-7, which is significantly lower than that of the lower continental crust, or lower crust-derived melts (Th/U = 3–50) in the Dabie Orogen (Ling et al., 2011). More recently, He et al. (2011) demonstrated that the early Cretaceous high Sr/Y granitoids (HSG) from the Dabie Orogen were generated by high-pressure partial melting of the thickened (>50 km) LCC. These HSG are characterized by higher Sr and Sr/CaO at given SiO_2 than the normal calc-alkaline rocks. It is noted that the LYRB rocks of this study are similar to the normal calc-alkaline rocks, rather than the HSG, on the Sr vs. SiO_2 and Sr vs. CaO diagrams (Fig. 11). Overall, the integrated geological, geochemical and isotopic observations argue against a LCC origin for the LYRB adakitic rocks.

5.2.2 Melting of subducted oceanic crust model

An alternative model for the generation of the LYRB "adakitic" rocks by melting of subducted oceanic slab was proposed based on the following arguments. (1) Ling et al. (2011) demonstrated that the LYRB "adakitic" rocks have a restricted range of Th/U ratios (mostly around 3–6), which is consistent with our new data for the Jiurui and Edong rocks with Th/U = 2.9–7.0 and a mean of 4.5 $\pm$ 1.2 (1σ) (Appendix Table 2). Such a range of Th/U ratios is consistent with that of oceanic crust-generated melts (Th/U $\approx$ 3), but significantly lower than that of the lower continental crust or its derived melts, or lower crust-derived adakitic rocks (Th/U = 3–50), in the Dabie Orogen (Ling et al., 2011). (2) The LYRB ore-bearing 'adakitic" rocks have relatively

lower and more restricted La/Yb (14–49) and Sr/Y (29–185) ratios than those of the Dabie adakitic rocks (La/Yb = 21–402, Sr/Y = 6.5–1300), consistent with them being slab-derived and lower continental crust-derived adakites, respectively (Liu et al., 2010; Ling et al., 2011). (3) Liu et al. (2010) demonstrated that the LYRB ore-bearing adakitic rocks from Yueshan and Tongguanshan have more radiogenic Pb isotopes ($^{206}Pb/^{204}Pb$ = 17.74–17.90, $^{207}Pb/^{204}Pb$ = 15.48–15.55, and $^{208}Pb/^{204}Pb$ = 37.94–38.06) than those ($^{206}Pb/^{204}Pb$ = 16.26–16.38, $^{207}Pb/^{204}Pb$ = 15.34–15.40, and $^{208}Pb/^{204}Pb$ = 36.56–36.90) of the barren adakitic rocks from the STLF (South Tan-Lu Fault including Dabieshan). The less radiogenic Pb of the STLF adakites are consistent with that of the ancient lower continental crust of the Yangtze Craton, whilst the more radiogenic Pb of the LYRB adakitic rocks overlap with those of MORB. These authors interpreted that the continental crust-like Sr-Nd isotopes of the LYRB rocks are attributed to involvement of sediments in the magma source, and the LYRB ore-bearing adakitic rocks therefore represent partial melts of a hydrous oceanic crust with sediments.

Our integrated in-situ zircon Hf-O isotopic data, together with whole-rock geochemical and Sr-Nd isotopic data, however, do not support such an interpretation. Apart from a few analyses, the LYRB "adakitic" rocks have zircon $\delta^{18}O$ values mostly between 6.5‰ and 8.0‰ (Fig. 3). Taking into account of the SiO_2 contents of the host rocks and using the equation of $\delta^{18}O_{WR} \approx \delta^{18}O_{Zir} + 0.0612$ (wt.% SiO_2) – 2.5 (Valley et al., 2005), the $\delta^{18}O$ values for the ore-barren and ore-bearing magmas are calculated at 7.2–9.3‰ and 8.0–9.5‰, respectively. Slightly higher magmatic $\delta^{18}O$

530 values in the ore-bearing rocks than the barren ones might be attributed to fractional
531 crystallization of hornblende, titanite and magnetite (as these minerals have lower
532 $\delta^{18}O$ values than the equilibrium melt). Contamination of upper crustal materials is
533 negligible, as only two xenocrystic zircons are found among 222 dated zircons (Li XH
534 et al., 2010). Therefore, the oxygen isotopic compositions are mainly reflective of the
535 nature of their sources. It is noted that the calculated magmatic $\delta^{18}O$ values are clearly
536 lower than that of the partial melts of the basaltic rocks and/or sediments at the upper
537 part of a oceanic crust that typically have $\delta^{18}O$ values of ca. 9–20‰, but significantly
538 higher than that of melts from hydrothermally altered gabbros at the interior of an
539 oceanic crust which typically have $\delta^{18}O$ values of ca. 2–5‰ (Bindeman et al., 2005).
540 While the oxygen isotopic compositions could be attributed to mixing of the upper
541 and interior/lower oceanic crust portions, several lines of evidence argue against this
542 possibility. First, the continental crust-like whole-rock Sr-Nd and zircon εHf isotopic
543 compositions of the LYRB rocks are clearly inconsistent with their predominant
544 derivation from oceanic crust. Second, the LYRB "adakitic" rocks are
545 characteristically potassium-rich, in contrast to the oceanic crust-derived melts that
546 are potassium-depleted. Third, lack of correlations between the whole-rock Sr-Nd
547 isotopes and geochemistry (not shown) is inconsistent with the binary mixing process.
548 Forth, magmatic $\delta^{18}O$ values of the LYRB "adakitic" rocks are clearly higher than
549 those ($\delta^{18}O$ = 6.4–7.3‰) of typical slab-derived adakites whose compositions could
550 be a result of a mixture of the slab sources in terms of oxygen isotopes (Bindeman et
551 al., 2005). Our geochemical modeling results confirm that fractional crystallization

552 played a major role in magmatic processes of these rocks, which accounts for their
553 "adakitic" geochemical features (e.g. high Sr/Y and La/Yb). Therefore, the integrated
554 isotopic and geochemical data do not support the interpretation that the LYRB
555 adakitic rocks resulted from partial melts of the subducted oceanic crust.
556
557 **5.2.3 Melting of a subduction-enriched mantle source model**
558 As noted, the parental magmas of the barren rocks are likely potassium-rich
559 basalt to basaltic andesite in compositions, which are usually considered to be derived
560 from a mantle enriched by subduction-related metasomatism (e.g., Müller and Groves,
561 1995). This is consistent with the interpretation of J.W. Li et al. (2009) who suggested
562 that the Edong plutonic rocks were derived from an enriched mantle source. The
563 continental crust-like Sr and Nd isotopic compositions of these rocks (Fig. 8) are
564 indistinguishable from those of the regional Cretaceous basalts (Xie et al., 2006b),
565 likely reflective of the isotopic compositions of their mantle sources. Figure 12 shows
566 a comparison of the calculated magmatic $\delta^{18}O$ values of the LYRB "adakitic" rocks
567 with the world's island arc volcanic rocks, adakites, high-Mg andesites,
568 geochemically exotic melts from Setouchi (Japan), and Archean orogenic TTGs and
569 post-orogenic sanukitoids (compiled by Bindeman et al., 2005). Inferred magmatic
570 $\delta^{18}O$ values of the LYRB adakitic rocks are not only considerably higher than those of
571 mid-ocean ridge basalts (MORB) (5.5-5.8‰) and island arc volcanic rocks
572 (5.7-6.4‰), but also clearly higher than those of slab-derived adakites (6.4-7.3‰),
573 TTG suites (6.3-7.4‰) and high-Mg andesites (HMAs) (6.8-7.7‰). On the other

574 hand, their magmatic $\delta^{18}O$ values, particularly those of the barren rocks, largely
575 overlap those of the Setouchi lavas (6.8-8.2‰) in SW Japan and the Archrean
576 post-orogenic sanukitoids (7.3-8.8‰).

577 Figure 13 compares the K_2O/Na_2O, Sr and Rb+Ba compositions of some high
578 Sr/Y rocks (including slab-melt adakites, Archrean post-orogenic sanukitoids, the
579 Setouchi high-Mg andesites and high Ba-Sr granites) with that of the LYRB
580 "adakitic" rocks of this study. Slab-melt adakites are characteristically high in Sr but
581 low in K_2O/Na_2O and Rb+Ba, whereas Archrean sanukitoids, high Ba-Sr granites and
582 the Setouchi lavas are relatively higher in K_2O/Na_2O and Rb+Ba and lower in Sr than
583 the slab-melt adakites. The term "sanukitoid" was coined by Shirey and Hanson (1984)
584 to describe a suite of Late Archaean diorites to granodiorites from the Superior
585 Province that display similar major element geochemistry to the Miocene high-Mg
586 andesite (sanukite) from the Setouchi volcanic belt of Japan (e.g., Tatsumi and
587 Ishizaka, 1982). In general, sanukitoids have intermediate major and trace element
588 compositions between typical Archaean TTG and modern arc granitoids. They are
589 characterized by high Mg# (>70), high Ni and Cr contents; Ba > 800 ppm; Sr > 800
590 ppm, enrichment in alkali ($Na_2O + K_2O > 3\%$ for $SiO_2 = 50\%$) and strongly
591 fractionated REE patterns ($Ce_N/Yb_N = 10–50$, $Ce_N > 100$) (Moyen et al., 2003;
592 Martin et al., 2009). The genesis for sanukitoids is often thought to be linked, directly
593 or indirectly, to TTG melts derived from partial melting of basaltic crust in two
594 scenarios: (1) TTG melts react with peridotite to give a sanukitoid liquid; (2) TTG
595 melts are entirely consumed by metasomatic reactions with the peridotite, and

596 subsequent malting of the metasomatized mantle results in sanukitoids (e.g., Martin et
597 al., 2009; Laurent et al., 2011). The Setouchi high-Mg andesite lavas were considered
598 to be modern analogues of the Archean sanukitoids (Tomlinson et al., 2002). They
599 have lower Sr/Y and La/Yb ratios, but much higher magmatic $\delta^{18}O$ (6.8-8.2‰) and
600 initial I_{Sr} (0.7041-0.7060) values than those of typical adakites and high-Mg andesites,
601 suggesting addition of silicic melt from subducted sediments to their peridotite mantle
602 sources (e.g., Tatsumi 2001; Bindeman et al., 2005). High Ba-Sr granites are
603 generally associated with coeval appinites; they are considered to be formed by AFC
604 (assimilation-fractional crystallization) process of evolved appinite magmas that were
605 derived from enriched mantle sources metasomatised by previous subduction (e.g.,
606 Fowler and Henney, 1996; Ye et al., 2008). Such enriched mantle sources in the
607 Caledonian Orogen of northern Scotland are characteristically high in initial I_{Sr}
608 (~0.7061) and $\delta^{18}O$ (~8‰) (Fowler and Henney, 1996).

609 The LYRB "adakitic" rocks are generally comparable with the Archrean
610 sanukitoids, high Ba-Sr granites and the Setouchi lavas in terms of K_2O/Na_2O, Sr and
611 Rb+Ba compositions. Overall, they share similar geochemical and isotopic
612 compositions with the Archrean sanukitoids, high Ba-Sr granites and the Setouchi
613 lavas, but differ from slab-derived adakites. Similar to Archrean sanukitoids, the
614 Setouchi lavas and high Ba-Sr granites, the LYRB "adakitic" rocks display typical
615 continental crust-like isotopic compositions: high initial I_{Sr} (0.7054 to 0.7085) and
616 magmatic $\delta^{18}O$ (7.2–9.5‰) and low εNd(T) (–3.9 to –7.7) and zircon εHf(T) = 0.5 to
617 –12 (Appendix Table 1 and 3). These isotopic features suggest a significant

involvement of continental crustal materials in the magma by either crustal contamination or source-contamination. We use an I_{Sr} *vs.* magmatic $\delta^{18}O$ plot (Fig. 14) (James, 1981) to distinguish these two different possibilities. It can be seen that the Caledonian high Ba-Sr granites from northern Scotland display crustal contamination trend, i.e., $\delta^{18}O$ increases quickly with small increase of I_{Sr}, implying a crustal contamination process for their genesis (Fowler and Henney, 1996). On the contrary, the LYRB rocks and the Setouchi lavas form a coherent positive correlation; their I_{Sr} increases quickly with slight increases in $\delta^{18}O$ (Fig. 14). It is noteworthy that magmatic fractionation could result in oxygen isotopic fractionation. However, ~5% SiO_2 difference between the ore-bearing and barren rocks only causes ~0.3‰ difference in their magmatic $\delta^{18}O$ values on the basis of the quantitative correlation of $\delta^{18}O_{WR} \approx \delta^{18}O_{Zir} + 0.0612$ (wt.% SiO_2) – 2.5 (Valley et al., 2005). Such small difference could not change the Sr-O isotopic trend of source-contamination. This is consistent with the genesis of the Setouchi lavas whose mantle source was contaminated by sedimentary melts (Bindeman et al., 2005). Therefore, the continental crust-like isotopic signatures in the LYRB adakitic rocks can best be attributed to source-contamination, whereas crustal contamination played little, if any, role in their genesis. Compared with the Setouchi lavas, the LYRB rocks have higher $\delta^{18}O$ and I_{Sr} values, possibly reflecting the involvement of a larger fraction of sedimentary melts in their mantle source.

In summary, we conclude that the parental magmas of the LYRB ore-barren intrusive rocks were derived from an enriched mantle source that had been

metasomatised by sedimentary melts. Ore-bearing “adakitic” porphyries were generated by fractional crystallization of the barren magmas with little, if any, crustal contamination. Fractional crystallization of hornblende, titanite, magnetite and apatite from the melts resulted in the adakite-like geochemical features such as high Sr/Y and La/Yb in the ore-bearing porphyries. This petrogenesis has significant implications for the mechanism of Cu-Au mineralization in the differentiated felsic rocks, though it is beyond the scope of present study. Relatively high Sr/Y and La/Yb characteristics of the ore-bearing porphyries reflect the hydrous and evolved nature of these rocks through hornblende + titanite over plagioclase fractionation. The mineral assemblage of hornblende, biotite, magnetite, apatite and titanite suggest a high oxidization state for the origin of these rocks. Thus, we consider that the mineralization is likely attributed to fractional crystallization, with or without crustal assimilation, of high-K calc-alkaline basaltic andesite magmas sourced by partial melting of the metasomatized mantle wedge under hydrous, oxidized condition, which is highly advantageous to Cu-Au metallogenesis (Richards and Kerrich, 2007).

5.3 Regional tectonic implications: flat-slab subducton or ocean-ridge subduction?

Mesozoic magmatism, including the LYRB magmatism, is widespread in eastern South China (Fig. 15) and present a rich source for W-Sn-Mo-Bi-Be-Nb-Ta and Cu-Fe-Au-Mo-Zn-Pb-Ag mineral deposits (e.g., Chang et al., 1991; Zhai et al., 1992; Pei and Hong, 1995). However, the tectonic driver that caused such an intracontinental large magmatic province has been an enigma for many years. The

traditional wisdom was that the magmatic province represent a continental magmatic arc (e.g., Jahn et al., 1990). However, the ca. 1000 km width of the magmatic province, and their complex chemical/petrological compositions (i.e. the presence of large amount of A-type granites and other extensional continental magmatism, with only a minor amount of andesite) argue against a simple arc model (Li, 2000; Li and Li, 2007). Zhou and Li (2000) recognize a coastward younging trend in the Jurassic-Cretaceous magmatism in the eastern half of the magmatic province, and proposed that the subduction angle changed from shallow to steep in that time interval. However, the model explains neither the western half of the magmatic province, nor the non-arc characteristics of the bulk of the magmatism or the pre-Jurassic magmatism.

Li and Li (2007) proposed a flat-slab subduction to explain (1) the propagation of a Permian-Triassic orogenic front from the coastal region to ca. 1300 km into the continental interior, featuring a widening fold-and-thrust belt with a small amount of syn-orogenic magmatism, and (2) the development of a broad sag basin on top of the orogeny between late Triassic and early Jurassic. Their model suggests that the foundering of the flat-slab caused a post-orogenic magmatic flare-up that started from central-southern south China at ca. 190 Ma, and propagated to the entire southeastern China by ca. 90 Ma, accompanied by a crustal rebound and extension (see contours of post-orogenic magmatic front at 180 Ma, 160 Ma and 140 Ma, respectively, in Fig. 13 and Appendix 4 that shows the central and northern part of the Mesozoic magmatic province).

684 Cretaceous magmatism in the Dabie Orogen (Fig. 13) has in the past been
685 interpreted as a result of orogenic collapse after the collision between the South and
686 North China blocks (e.g., Li, 1994; Wu et al., 2007; Zhang et al., 2010). However, as
687 shown in Figure 13 and Appendix 4, the age distribution of Mesozoic magmatism in
688 both the Dabie Orogen, and the LYRB to its south and east, is consistent with the
689 broad outward-younging trend for the entire eastern south China. Their genesis may
690 thus be linked to the foundering of the flat-slab too.

691 We illustrate in Figure 16 how this may work. At ca. 200 Ma, near the end of the
692 Indosinian Orogeny caused by the initiation of the subduction along the coast (Li et
693 al., 2006) and then the flat-subductin of a young and hot oceanic plateau (Li and Li,
694 2007), continuing slow eclogization of the oceanic plateau at relatively low
695 temperatures drove the slow dewatering of the plateau basalts, which metasomatized
696 the subcontinental lithospheric mantle (Fig. 16A). At the same time, a section of the
697 normal oceanic lithosphere under the Dabie Orogen and the region to its east in the
698 LYRB, which traveled with the flat-slab all the way from the subduction zone >500
699 km away, had already gone through much of its dewatering process at that P-T
700 condition before reaching the Dabie mantle region, and was thus unable to drive
701 significant metasomatism of the rocks above it. The delamination of the flat-slab after
702 ca. 190 Ma (Fig. 16B) caused fast dewatering of the oceanic plateau and melting of
703 both some of the plateau basalts to generate the Dexing adakitic granites (Wang Q et
704 al. 2006b), and the metasomatised lithospheric mantle and mantle wedge to generate
705 the high-K calc-alkaline intrusive rocks in the study region. Melts of the sediments on

706 the oceanic plateau likely caused the enrichment in ^{87}Sr and ^{18}O of the metasomatised
707 mantle. At that time (ca. 170-140 Ma, Fig. 16B), little was happening in the mantle
708 beneath the Dabie Orogen and the region to its east.

709 After ca. 140 Ma, the entire subducted slab became detached from the continental
710 lithosphere (Fig. 16C). The increased pressure and elevated ambient mantle
711 temperature would have allowed further dehydration of the entire oceanic slab
712 (including a small amount of dewatering from the normal oceanic crust). This,
713 together with the heat conducted by the asthenospheric upwellings, would have driven
714 further melting above the foundering oceanic plateau. Similar conditions, together
715 with a thinned lithosphere due to orogenic erosion and orogenic collapse, would also
716 have driven the melting of the thickened lower crust under the Dabie Orogen to form
717 high Sr/Y granites (lower crust-derived barren adakitic rocks) at ca. 140-130 Ma (Fig.
718 16C), followed by emplacement of normal calc-alkaline granites and mafic-ultramafic
719 intrusions in response to removal of the eclogitic mountain root at ca. 130-120 Ma
720 (e.g., Li et al., 1999; Zhao et al., 2005; Liu et al., 2010; He et al., 2011).

721 As an alternative to the flat-slab foundering model, Ling et al. (2009) and Sun et
722 al. (2010) proposed a ridge subduction model for the generation of the LYRB
723 magmatism and related mineralization. However, such a model would predict a
724 younging trend of magmatism from the coastal region to the continental interior,
725 which is opposite to the trend as shown in Figure 15. In addition, the ridge-subduction
726 model predicts a slab window and formation of slab-derived adakites (Ling et al.,
727 2009). Slab windows formed by ridge-subduction have been identified as important

sites for slab melting, and adakitic melts form proximal to the slab window margins at depths of 25-90 km (e.g., Thorkelson and Breitsprecher, 2005). It is noted that most Cenozoic adakites related to ridge subduction were formed in the near-trench locations (Cole and Stewart, 2009). Contrarily, the spatial distribution of the LYRB "adakitic" rocks is broadly within the continental interior perpendicular to the continental margin. In particular, the "adakitic rocks" in the Edong mining district are >1000 km away from the present continental margin. Provided the "adakitic" rocks in the Edong were formed at depths of 25-90 km, it would invoke a flattened subduction with an angle of <5°. Considering the synchronous formation of adakitic rocks (X.H. Li et al., 2010) and development of rift basins (Zhu et al., 2010) along the whole LYRB, such a flat ridge subduction is unlikely feasible. Our integrated geochemical and isotopic data demonstrate that the studied "adakitic rocks" are most likely derived from the metasomatised mantle sources, rather than the subducting oceanic crust.

6 Conclusions

We draw the following conclusions based on our comprehensive analyses of situ zircon Hf-O isotopes and whole-rock geochemistry and Sr-Nd isotopes as well as regional geological data.

(1) The LYRB "C-type adakitic rocks" consist of monzodiorite, granodiorite and quartz monzonite. Characteristically high in potassium (K_2O = 2.4–4.5%, K_2O/Na_2O = 0.6–1.3), they belong to shoshonitic to high-K calc-alkaline series. The ore-bearing

and barren rocks are most likely cogenetic products of common parental magmas. Fractional crystallization of hornblende, titanite, magnetite and apatite plays a major role in their chemical variations, with the ore-bearing rocks being more felsic (SiO_2 = 63.3–69.6%) and higher in Sr/Y (41.2–75.6) and $(La/Yb)_N$ (17–50) than the barren rocks (SiO_2 = 57.3–65.0%, Sr/Y =30.4–51.8 and $(La/Yb)_N$ = 12–23). High Sr/Y and $(La/Yb)_N$ ratios of the ore-barren porphyries are more likely attributed to hornblende fractionation than their primary features formed by high-pressure melting with residual garnet ± hornblende ± clinopyroxene.

(2) The LYRB "C-type adakitic rocks" have typical continental crust-like isotopic compositions, i.e., whole-rock εNd(T) = –3.9 to –7.7, I_{Sr} = 0.7054 to 0.7085; zircon εHf(T) = 0 to –11, and zircon $\delta^{18}O$ = 6‰ to 9‰. Integration of geochemistry, zircon Hf-O and whole-rock Sr-Nd isotopes and regional geological data suggests that the LYRB "C-type adakitic rocks" are unlikely formed by either melting of thickened and/or delaminated lower crust, or altered oceanic crust as previously thought. They are akin in geochemistry and isotopes to the Archrean sanukitoids and the Setouchi high-Mg andesites, and most likely generated by melting of an enriched mantle source metasomatized by subduction processes. These potassium-rich rocks are genetically different from those sodic adakitic rocks generated by melting of eclogites and/or garnet amphibolites in the thickened, orogenic lower crust in Tibet (Chung et al., 2003) and Andes (Petford and Atherton, 1996). Thus, they could not be classified as the "C-type adakites" as previously thought.

(3) As the northern part of the Yanshanian intracontinental large magmatic

772 province in southeastern China, the model of flat-slab subduction of oceanic plateau
773 since early Mesozoic beneath southeastern China and subsequent delamination and
774 foundering of the flat-slab can best account for the formation of the metasomatised
775 mantle source for generating the LYRB potassium-rich intrusive rocks.
776
777 **Acknowledgement**

778 We thank Guo-Qiang Tang, Yu Liu, Yue-Heng Yang and Ying Liu for their
779 assistance in geochemical and isotope analyses. Comments from two anonymous
780 reviewers and the editor-in-chief Laurie Reisberg improved the paper greatly. This
781 work was supported by the Chinese Ministry of Science and Technology (grant
782 2012CB416702), the Chinese Academy of Sciences (grant KZCX2-YW-15-2), and
783 the Australian Research Council (DP110104799). This is TIGeR (The Institute for
784 Geoscience Research) publication xxx and contribution xxx from the ARC Centre of
785 Excellence for Core to Crust Fluid Systems.
786

References

Ames, L., Zhou, G.Z., Xiong, B.C., 1996. Geochronology and isotopic character of ultrahigh-pressure metamorphism with implications for collision of the Sino-Korean and Yangtze cratons, central China. Tectonics 15, 472-489.

Bachmann, O., Dungan, M.A., Bussy, F., 2005. Insights into shallow magmatic processes in large silicic magma bodies: the trace element record in the Fish Canyon magma body, Colorado. Contribut. Mineral. Petrol. 149, 338-349.

Bindeman, I.N., Eilerb, J.M., Yogodzinski, G.M., Tatsumi. Y., Stern, C.R., Grove, T.L., Portnyagin, M., Hoernle, K., Danyushevsky, L.V., 2005. Oxygen isotope evidence for slab-derived in modern and ancient subduction zones. Earth Planet. Sci. Lett. 235, 480-496.

Black, L.P., Kamo, S.L., Allen, C.M., Davis, D.W., Aleinikoff, J.N., Valley, J.W., Mundil, R., Campbel, I.H., Korsch, R.J., Williams, I.S., Foudoulis, Chris., 2004. Improved $^{206}Pb/^{238}U$ microprobe geochronology by the monitoring of a trace-element-related matrix effect; SHRIMP, ID-TIMS, ELA-ICP-MS and oxygen isotope documentation for a series of zircon standards. Chem. Geol. 205, 115-140.

Blichert-Toft, J., 2008. The Hf isotopic composition of zircon reference material 91500. Chem. Geol., 253, 252-257.

Castillo, P.R., 2006. An overview of adakite petrogenesis. Chi. Sci. Bull. 51, 258-268.

Castillo, P.R., 2012. Adakite petrogenesis. Lithos 134-135, 304-316.

Chang, Y.F., Liu, X.P., Wu, Y.C., 1991. The Copper–Iron Belt of the Lower and Middle Reaches of the Changjiang River. Geological Publishing House, Beijing, 379 pp (in Chinese with English abstract).

Choi, S.G., Rajesh, V.J., Seo, J., Park, J.W., Oh, C.W., Pakm S.J., Kim, S.W., 2009. Petrology, geochronology and tectonic implications of Mesozoic high Ba-Sr granites in the Haemi area, Hongseong Belt, South Korea. Island Arc, 18, 266-281.

Chung, S.L., Liu, D., Ji, J., Chu, M.F., Lee, H.Y., Wen, D.J., Lee, T.Y., Qian, Q.,

816 Zhang, Q., 2003. Adakites from continental collision zones: Melting of thickened
817 lower crust beneath southern Tibet. Geology, 31, 1021-1024.

818 Cocherie, A., 1986. Systematic use of trace-element distribution patterns in log-log
819 diagrams for plutonic suites. Geochim. Cosmochim. Acta 50, 2517-2522.

820 Cole, R.B., Steward, B.W., 2009. Continental margin volcanism at sites of spreading
821 ridge subduction: Examples from southern Alaska and western California.
822 Tectonophysics 464, 118-136.

823 Defant, M.J., Drummond, M.S., 1990. Derivation of some modern arc magmas by
824 melting of young subducted. lithosphere. Nature 367, 662-665.

825 Defant M. J., Xu J. F., Kepezhinskas P., Wang Q., Zhang Q., Xiao L., 2002. Adakites:
826 some variations on a theme. Acta Petrol. Sin. 18, 129-142.

827 Drummond, M.S., Defant, M.J., 1990. A model from trondhjemite–tonalite–dacite
828 genesis and crustal growth via slab-derived: Archaean to modern comparisons. J.
829 Geophys. Res. 95, 21503–21521.

830 Fowler, M.B., Henney, P.J., 1996. Mixed Caledonian appinite magmas: implications
831 for lamprophyre fractionation and high Ba-Sr granite genesis. Contrib. Minerl.
832 Petrol. 126, 199-215.

833 Gao, S., Ling, W.L., Qiu, Y.M., Lian, Z., Hartmann, G., Simon, K., 1999. Contrasting
834 geochemical and Sm-Nd isotopic compositions of Archean metasediments from
835 the Kongling high-grade terrain of the Yangtze craton: evidence for Cratonic
836 evolution and redistribution of REE during crustal anatexis. Geochim.
837 Cosmochim. Acta 63, 2071-2088.

838 Gao, S., Yang, J., Zhou, L., Li, M., Hu, Z., Guo, J., Yuan, H., Gong, H., Xiao, G., Wei,
839 J., 2011. Age and growth of the Archean Kongling terrain, South China, with
840 emphasis on 3.3 Ga granitoid gneisses. Am J. Sci., 311, 153-182.

841 Goolaerts, A., Mattielli, N., Jong, J.D., Weis, D, James, D., Scoates J.S., 2004. Hf and
842 Lu Isotopic reference values for the zircon standard 91500 by MC-ICP-MS.
843 Chem. Geol., 206, 1-9.

844 Grimmer, J.C., Ratschbacher, L., McWilliams, M., Franz, L., Gaitzsch, I.,
845 Tichomirowa, M., Hacker, B.R., Zhang, Y., 2003. When did the
846 ultrahigh-pressure rocks reach the surface? A $^{207}Pb/^{206}Pb$ zircon, $^{40}Ar/^{39}Ar$ white
847 mica, Si-in-white mica, single-grain provenance study of Dabie Shan synorogenic
848 foreland sediments. Chem. Geol. 197, 87-110.
849 He, Y.S., Li, S.G., Hoefs, J., Huang, F., Liu, S.A., Hou, Z.H., 2011. Post-collisional
850 granitoids from the Dabie orogen: New evidence for partial melting of a
851 thickened continental crust. Geochim. Cosmochim. Acta 75, 3815-3838.
852 Jahn, B.M., Zhou, X.H., Li, J.L., 1990. Formation and tectonic evolution of
853 Southeastern China and Taiwan: Isotopic and geochemical constraints.
854 Tectonophysics 183, 145-160.
855 James, D.E., 1981. The combined use of oxygen and radiogenic isotopes as indicators
856 of crustal contamination. Annu. Rev. Earth Planet. Sci. 9, 311-344.
857 Jiao, W.F., Wu, Y.B., Yang, S.H., Peng, M., Wang, J., 2009. The oldest basement rock
858 in the Yangtze Craton revealed by zircon U-Pb age and Hf isotope composition.
859 Sci. China Ser. D: Earth Sci. 52, 1393-1399.
860 Klein, M., Stosch, H.G., Seck, H.A., 1997. Partitioning of high field-strength and
861 rare-earth elements between amphibole and quartz-dioritic to tonalitic melts: an
862 experimental study. Chem. Geol. 138, 257-271.
863 Krogstad, E.J., Hanson, G.N., Rajamani, V., 1995. Sources of continental magmatism
864 adjacent to late Archaean Kolar suture zone, south India: distinct isotopic and
865 elemental signatures of two late Archaean magmatic series. Contrib. Mineral.
866 Petrol. 122, 159-173.
867 LaTourrette, T., Hervig, R.L., Holloway, J.R., 1995. Trace element partitioning
868 between amphibole, phlogopite, and basanite melt. Earth Planet. Sci. Lett. 135,
869 13-30.
870 Laurent, O., Martin, H., Doucelance, R., Moyen, J.F., Paquette, J.L., 2011.
871 Geochemistry and petrogenesis of high-K “sanukitoids” from the Bulai pluton,

872 Central Limpopo Belt, South Africa: Implications for geodynamic changes at the
873 Archaean–Proterozoic boundary. Lithos 123, 73-91.

874 Li, C.F., Li, X.H., Li, Q.L., Guo, J.H., Li, X.H., Yang, Y.H., 2012. Rapid and precise
875 determination of Sr and Nd isotopic ratios in geological samples from the same
876 filament loading by thermal ionization mass spectrometry employing a
877 single-step separation scheme. Anal. Chim. Acta 727, 54-60.

878 Li, J., Li, X., Pei, R., Mei, Y., Wang, Y., Qu, W., Huang, X., Zhan, W., 2007. Re-Os
879 age of molybdenite from the southern ore zone of the Wushan copper deposit,
880 Jiangxi Province and its geological significance. Acta Geol. Sinica, 81, 801-807.

881 Li, J.W., Zhao, X.F., Zhou, M.F., Vasconcelos, P., Ma, C.Q., Deng, X.D., de Souza,
882 Z.S., Zhao, Y.X., Wu, G., 2008. Origin of the Tongshankou porphyry-skarn
883 Cu-Mo deposit, eastern Yangtze craton, Eastern China: geochronological,
884 geochemical, and Sr-Nd-Hf isotopic constraints. Mineral. Dep. 43, 315-336.

885 Li, J.W., Zhao, X.F., Zhou, M.F., Ma, C.Q., de Souza, Z.S., Vasconcelos, P., 2009.
886 Late Mesozoic magmatism from the Daye region, eastern China: U-Pb ages,
887 petrogenesis, and geodynamic implications. Contrib. Mineral. Petrol. 157,
888 383-409.

889 Li, S.G., Hong, J.A., Li, H.M., Jiang, L.L., 1999. Zircon U-Pb dating of
890 pyroxenite–gabbro intrusions in the Dabie orogen and their geological
891 implications. Geol. J. Chinese Univ. 5, 351-355 (in Chinese with English
892 abstract).

893 Li, X.H., 2000, Cretaceous magmatism and lithospheric extension in Southeast China.
894 J. Asian Earth Sci. 18, 293-305.

895 Li X.H., Sun M., Wei G.J., Liu Y., Lee C.Y., Malpas J.G., 2000, Geochemical and
896 Sm-Nd isotopic study of amphibolites in the Cathaysia Block, SE China:
897 evidence for extremely depleted mantle in the Paleoproterozoic. Precambrian Res.
898 102, 251-262.

899 Li, X.H., Qi, C.S., Liu, Y., Liang, X.R., Tu, X.L., Xie, L.W., Yang, Y.H., 2005.

Petrogenesis of the Neoproterozoic bimodal volcanic rocks along the western margin of the Yangtze Block: new constraints from Hf isotopes and Fe/Mn ratios. Chi. Sci. Bull. 50, 2481-2486.

Li, X.H., Li, Z.X., Li, W.X., Wang, Y.J., 2006. Initiation of the Indosinian Orogeny in South China: Evidence for a Permian magmatic arc on Hainan Island. J. Geology 114, 341-353.

Li, X.H., Li, W.X., Wang, X.C., Li, Q.L., Liu, Y., Tang, G.Q., Gao, Y.Y., Wu, F.Y., 2010a. SIMS U–Pb zircon geochronology of porphyry Cu–Au–(Mo) deposits in the Yangtze River Metallogenic Belt, eastern China: Magmatic response to early Cretaceous lithospheric extension. Lithos, 119, 427-438.

Li, X.H., Li, W.X., Li, Q.L., Wang, X.C., Liu, Y., Yang, Y.H., 2010b. Petrogenesis and tectonic significance of the ~850 Ma Gangbian alkaline complex in South China: evidence from in-situ zircon U-Pb and Hf-O isotopes and whole-rock geochemistry. Lithos, 114, 1-15.

Li, Z.X., 1994. Collision between the North and South China Blocks - a crustal-detachment model for suturing in the region east of the Tanlu Fault. Geology 22, 739-742.

Li, Z.X., Li, X.H., 2007. Formation of the 1300-km-wide intracontinental orogen and postorogenic magmatic province in Mesozoic South China: A flat-slab subduction model. Geology 35, 179-182.

Ling, M.X., Wang, F.Y., Ding, X., Hu, Y.H., Zhou, J.B., Zartman, R.E., Yang, X.Y., Sun, W.D., 2009. Cretaceous ridge subduction along the lower Yangtze River belt, eastern China. Econ. Geol. 104, 303-321.

Ling, M.X., Wang, F.Y., Ding, X., Zhou, J.B., Sun, W.D., 2011. Different origins of adakites from the Dabie Mountains and the Lower Yangtze River Belt, eastern China: geochemical constraints. Int. Geol. Rev. 53, 727-740.

Liu, S.A., Li, S.G., He, Y.S., Huang, F., 2010. Geochemical contrasts between early Cretaceous ore-bearing and ore-barren high-Mg adakites in central-eastern China: Implications for petrogenesis and Cu-Au mineralization. Geochim. Cosmochim.

Acta 74, 7160-7178.

Machado, N., Simonetti, A., 2001. U–Pb dating and Hf isotopic composition of zircons by laser ablation-MC-ICP-MS. In: Sylvester, P. (Ed.), Laser-Ablation-ICPMS in the Earth Sciences: Principles and Applications. Short Course of Mineral. Assoc. Canada, 29, 121-146.

Mao, J.W., Wang, Y.T., Lehmann, B., Yu, J.J., Du, A.D., Mei, Y.X., Li, Y.F., Zang, W.S., Stein, H.J., Zhou, T.F., 2006. Molybdenite Re–Os and albite $^{40}Ar/^{39}Ar$ dating of Cu–Au–Mo and magnetite porphyry systems in the Yangtze River valley and metallogenic implications. Ore Geol. Rev. 29, 307-324.

Martin, H., Moyen, J.F., Rapp, R.P., 2009. The sanukitoid series: magmatism at the Archaean–Proterozoic transition. Earth and Environmental Science Transactions of the Royal Society of Edinburgh 100, 15-33.

Middlemost, E.A.K., 1994. Naming materials in the magma/igneous rock system. Earth-Sci. Rev. 37, 215-224.

Moyen, J. F., Martin, H., Jayananda, M., Auvray, B., 2003. Late Archaean granites: a typology based on the Dharwar Craton (India). Precambrian Res. 127, 103–23.

Müller, D., Groves, D., 1993, Direct and indirect associations between potassic igneous rocks, shoshonites, and gold-copper deposits. Ore Geol. Rev. 8, 383-406.

Pan, Y., Dong, P., 1999. The Lower Changjiang (Yangzi/Yangtze River) metallogenic belt, east central China: intrusion- and wall rock-hosted Cu-Fe-Au, Mo, Zn, Pb, Ag deposits. Ore Geol. Rev. 15, 177-242.

Peccerillo, A., Taylor, S.R., 1976. Geochemistry of Eocene calkalkaline volcanic rocks from the Kastamonu area, northern Turkey. Contrib. Miner. Petrol. 58, 61-83.

Pei, R, Hong, D., 1995. The granites of South China and their metallogeny. Episodes, 18, 77-82.

Petford, N., Atherton, M., 1996. Na-rich partial melts from newly underplated basaltic

crust: the Cordillera Blanca Batholith, Peru. J. Petrol. 37, 1491-1521.

Prowatke, S., Klemme, S., 2005. Effect of melt composition on the partitioning of trace elements between titanite and silicate melt. Geochim. Cosmochim. Acta 69, 695-709.

Qian, Q., Chung, S.L., Lee, T.Y., Wen, D.J., 2003. Mesozoic high-Ba–Sr granitoids from North China: geochemical characteristics and geological implications. Terra Nova 15, 272-278.

Raczek, I., Jochum, K.P., Hofmann, A.W., 2003. Neodymium and strontium isotope data for USGS reference materials BCR-1, BCR-2, BHVO-1, BHVO-2, AGV-1, AGV-2, GSP-1, GSP-2 and eight MPI-DING reference glasses. Geostand. Geoanal. Res. 27, 173-179.

Rapp, R., Xiao, L., Shimizu, N., 2002. Experimental constraints on the origin of potassium-rich adakites in eastern China. Acta Petrol. Sinica 18, 293-302.

Richards, J.R., Kerrich, R., 2007. Special paper: Adakite-like rocks: their diverse origins and questionable role in metallogenesis. Econ. Geol. 102, 537-576.

Rudnick, R.L., Gao, S., 2003. Composition of the continental crust, in Holland, H.D., and Turekian, K.K. (Eds.), Treatise on geochemistry, Volume 3: Oxford, Elsevier, pp. 1-64.

Bachmann, O., Dungan, M.A., Bussy, F., 2005. Insights into shallow magmatic processes in large silicic magma bodies: the trace element record in the Fish Canyon magma body, Colorado. Contributions to Mineralogy and Petrology, 149(3): 338-349.

Klein, M., Stosch, H.G., Seck, H.A., 1997. Partitioning of high field-strength and rare-earth elements between amphibole and quartz-dioritic to tonalitic melts: an experimental study. Chemical Geology, 138(3–4): 257-271.

LaTourrette, T., Hervig, R.L., Holloway, J.R., 1995. Trace element partitioning between amphibole, phlogopite, and basanite melt. Earth and Planetary Science Letters, 135(1–4): 13-30.

Prowatke, S., Klemme, S., 2005. Effect of melt composition on the partitioning of

985 trace elements between titanite and silicate melt. Geochimica et Cosmochimica
986 Acta, 69(3): 695-709.
987 Richards, J.P., Kerrich, R., 2007. Special Paper: Adakite-Like Rocks: Their Diverse
988 Origins and Questionable Role in Metallogenesis. Economic Geology, 102(4):
989 537-576.
990 Sisson, T.W., 1994. Hornblende-melt trace-element partitioning measured by ion
991 microprobe. Chem. Geol. 117, 331-344.
992 Shirey, S.B., Hanson, G.N., 1984. Mantle derived Archaean monzodiorites and
993 trachyandesites. Nature 310, 222-224.
994 Shimoda, G., Tatsumi, Y., Nohda, S., Ishizaka, K., Jahn, B.M., 1998. Setouchi
995 high-Mg andesites revisited: geochemical evidence for melting of subducting
996 sediments. Earth Planet. Sci. Lett. 160, 479-492.
997 Smithies, R.H., Champion, D.C., 1999. Late Archaean felsic alkaline igneous rocks in
998 the Eastern Goldfields, Yilgarn Craton, Western Australia: a result of lower
999 crustal delamination? J. Geol. Soc. London 156, 561-576.
1000 Stevenson, R., Henry, P., Gariépy, C., 1999. Assimilation-fractional crystallization
1001 origin of Archaean sanukitoid suites: Western Superior Province, Canada.
1002 Precambrian Res. 96, 83-99.
1003 Sun, S.S., McDonough, W.F., 1989. Chemical and isotopic systematics of oceanic
1004 basalt: implications for mantle composition and processes. In: Saunders, A.D.,
1005 Norry, M.J. (Eds.), Magmatism in the Ocean Basins. Geological Society Special
1006 Publication, No. 42, pp. 528-548.
1007 Sun W.D., Ling, M.X., Yang, X.Y. Fan, W.M., Ding, X., Liang, H., 2010. Ridge
1008 subduction and porphyry copper-gold mineralization: An overview. Sci. China
1009 Ser. D: Earth Sci 53, 475-484.
1010 Tatsumi, Y., Ishizaka, K., 1982. Origin of high-magnesian andesites in the Setouchi
1011 volcanic belt, southwest Japan: I. Petrographical and chemical characteristics.
1012 Earth Planet. Sci. Lett. 60, 293-304.
1013 Tatsumi, Y., 2001. Geochemical modeling of partial melting of subducting sediments
1014 and subsequent melt-mantle interaction: Generation of high-Mg andesites in the

Setouchi volcanic belt, southwest Japan. Geology 29, 323-326.

Thorkelson, D.J., Breitsprecher, K., 2005. Partial melting of slab window margins: genesis of adakitic and non-adakitic magmas. Lithos 79, 25-41.

Tomlinson, K.Y., Davis, D.W., Percival, J.A., Hughes, D.J., Thurston, P.C., 2002. Mafic to felsic magmatism and crustal recycling in the Obonga Lake greenstone belt, western Superior Province: evidence from geochemistry, Nd isotopes and U-Pb geochronology. Precambrian Res. 114, 295-325.

Valley, J.W., Lackey, J.S., Cavosie, A.J., Clechenko, C.C., Spicuzza, M.J., Basei, M.A.S., Bindeman, I.N., Ferreira, V.P., Sial, A.N., King, E.M., Peck, W.H., Sinha, A.K., Wei, C.S., 2005. 4.4 billion years of crustal maturation: oxygen isotope ratios of magmatic zircon. Contrib. Mineral. Petrol. 150, 561-580.

Wang, Q., Xu J.F., Zhao, Z.H., Bao, Z.W., Xu, W., Xiong, X.L., 2004a. Cretaceous high-potassium intrusive rocks in the Yueshan–Hongzhen area of east China: adakites in an extensional tectonic regime within a continent. Geochem. J. 38, 417-434.

Wang, Q., Zhao, Z.H., Bao, Z.W., Xu, J.F., Liu, W., Li, C.F., Bai, Z.H., and Xiong, X.L., 2004b, Geochemistry and petrogenesis of the Tongshankou and Yinzu adakitic intrusive rocks and the associated porphyry copper–molybdenum mineralization in southeast Hubei, east China. Resource Geol. 54, 137-152.

Wang, Q., Zhao, Z.H., Xu, J.F., Bai, Z.H., Wang, J.X., and Liu, C.X., 2004c. The geochemical comparison between the Tongshankou and Yinzu adakitic intrusive rocks in southeastern Hubei: (delaminated) Lower crustal melting and the genesis of porphyry copper deposit. Acta Petrol. Sinica 20, 351-360.

Wang, Q., Wyman, D.A., Xu, J.F., Zhao, Z.H., Jian, P., Xiong, X.L., Bao, Z.W., Li, C.F., Bai, Z.H., 2006a. Petrogenesis of Cretaceous adakitic and shoshonitic igneous rocks in the Luzong area, Anhui Province (eastern China): Implications for geodynamics and Cu-Au mineralization. Lithos, 89, 424-446.

Wang, Q., Xu, J.F., Jian, P., Bao, Z.W., Zhao, Z.H., Li, C.F., Xiong, X.L., Ma, J.L., 2006b. Petrogenesis of adakitic porphyries in an extensional tectonic setting,

Dexing, South China: implications for the genesis of porphyry copper mineralization. J. Petrol. 47, 119-144.

Wang Q., Wyman D. A., Xu J. F., Zhao Z. H., Jian P. and Zi F., 2007. Partial melting of thickened or delaminated lower crust in the middle of eastern China: implications for Cu-Au mineralization. J. Geol. 115, 149-161.

Wiedenbeck, M., Hanchar, J.M., Peck, W.H., Sylvester, P., Valley, J., Whitehouse, M., Kronz, A., Morishita, Y., Nasdala, L., Fiebig, J., Franchi, I., Girard, J.P., Greenwood, R.C., Hinton, R., Kita, N., Mason, P.R.D., Norman, M., Ogasawara, M., Piccoli, R., Rhede, D., Satoh, H., Schulz-Dobrick, B., Skar, O., Spicuzza, M.J., Terada, K., Tindle, A., Togashi, S., Vennemann, T., Xie, Q., Zheng, Y.F., 2004. Further characterisation of the 91500 zircon crystal. Geostand. Geoanal. Res. 28, 9-39.

Wu, F.Y., Yang, Y.H., Xie, L.W., Yang, J.H., Xu, P., 2006. Hf isotopic compositions of the standard zircons and baddeleyites used in U-Pb geochronology. Chem. Geol. 234, 105-126.

Wu, F.Y., Yang, Y.H., Marks, M.A.W., Liu, Z.C., Zhou, Q., Ge, W.C., Yang, J.S., Zhao, Z.F., Mitchell, R.H., Markl,G., 2010. In situ U–Pb, Sr, Nd and Hf isotopic analysis of eudialyte by LA-(MC)-ICP-MS. Chem. Geol. 273, 8-34.

Wu, Y.B., Zheng, Y.F., Zhang, S.B., Zhao, Z.F., Wu, F.Y., Liu, X.M., 2007. Zircon U–Pb ages and Hf isotope compositions of migmatite from the North Dabie terrane in China: constraints on partial melting. J. Metamorph. Geol. 25, 991-1009.

Xiao, L. and Clemens, J.D., 2007. Origin of potassic (C-type) adakite magmas: Experimental and field constraints. Lithos, 95, 399-414.

Xie, G.Q., Mao, J.W., Li, R.L., Zhang, Z.S., Zhao, W.,C., Qu, W.J., Zhao, C.S., Wei, S.K., 2006a. Metallogenic epoch and geodynamic framework of Cu-Au-Mo-(W) deposits in Southeastern Hubei Province: constraints from Re-Os molybdenite ages. Mineral Deposita 25, 43-52.

Xie, G.Q., Mao, J.W., Li, R., Zhou, S.D., Ye, H.R., Yan, Q.R., Zhang, Z.S., 2006b. SHRIMP U–Pb age of the Dasi Formation volcanic rocks from southeastern

Hubei, mid-lower reaches of the Yangtze River. Sci China Ser. D 51, 2283-2291.

Xu, J.F., Shinjo, R., Defant, M.J., Wang, Q., Rapp, R.P., 2002. Origin of Mesozoic adakitic intrusive rocks in the Ningzhen area of east China: Partial melting of delaminated lower continental crust? Geology 30, 1111-1114.

Yang, J.H., Chung, S.L., Zhai, M.G., Zhou, X.H., 2004. Geochemical and Sr-Nd-Pb isotopic compositions of mafic dikes from the Jiaodong Peninsula, China: evidence for vein-plus-peridotite melting in the lithospheric mantle. Lithos 73, 145-160.

Ye, H.M., Li, X.H., Li, Z.X., Zhang, C.L., 2008. Age and origin of high Ba-Sr appinite-granites at the northwestern margin of the Tibet Plateau: Implications for early Paleozoic tectonic evolution of the Western Kunlun orogenic belt. Gondwana Res., 13 126-138.

Zhang Q., Wang Y., Qian Q., Yang J. H., Wang Y. L., Zhao T. P. and Guo G. J., 2001. The characteristics and tectonic-metallogenic significances of the adakites in Yanshan period from eastern China. Acta Petrol. Sinica 17, 236-244.

Zhang, J., Zhao, Z.F., Zheng, Y.F., Dai, M., 2010. Postcollisional magmatism: Geochemical constraints on the petrogenesis of Mesozoic granitoids in the Sulu orogen, China. Lithos 119, 512-536.

Zhai, Y.S., Yao, S.Z., Lin, X.D., Zhou, X.N., Wan, T.F., Jin, F.Q., Zhou, Z.G., 1992. Fe-Cu-(Au) metallogeny of the Middle–Lower Changjiang region. Geological Publishing House, Beijing, 235 pp (in Chinese).

Zhao, Z.F., Zheng, Y.F., Wei, C.S., Wu, Y.B., Chen, F.K., Jahn, B.M., 2005. Zircon U-Pb age, element and C-O isotope geochemistry of post-collisional mafic–ultramafic rocks from the Dabie orogen in east-central China. Lithos 83, 1-28.

Zhou, T.F., Fan, Y., Yuan, F., Lu, S.M., Shang, S.G., David, C., Sebastien, M., Zhao, G.C., 2008. Geochronology of the volcanic rocks in the Lu-Zong basin and its significance. Sci. China Ser. D: Earth Sci. 51, 1470-1482.

Zhou, X.M., Li, W.X., 2000. Origin of Late Mesozoic igneous rocks in Southeastern

China: implications for lithosphere subduction and underplating of mafic magmas. Tectonophysics 326, 269-287.

Zhu, G., Niu, M., Xie, C., Wan, Y., 2010. Sinistral to Normal Faulting along the Tan-Lu Fault Zone: Evidence for Geodynamic Switching of the East China Continental Margin. J. Geol. 118, 277-293.

Figure captions

Fig. 1 (A) a tectonic sketch of China; (B) simplified geologic map of the central-eastern China showing the distribution of latest Jurassic to early Cretaceous adakititic rocks, modified after Wang et al. (2007) and Liu et al. (2010); (C) distribution of adakititic rocks in the southern Edong mining district; (D) distribution of adakititic rocks in the Jiurui mining district. TLF = Tan-Lu Fault; JSF = Jiang-Shao Fault; TSK = Tongshankou.

Fig. 2 Harker-type chemical variation diagrams for the Jiurui and Edong "adakitic" plutonic rocks. The fields of metabasaltic and eclogite experimental melts and subducted oceanic crust-derived adakites in the SiO_2 *vs.* MgO plot are after a compilation by Q. Wang et al. (2006a).

Fig. 3 (A) Total alkali vs. silica (TAS) diagram, and (B) K_2O vs. SiO_2 diagram for the Jiurui and Edong "adakitic" plutonic rocks. The calc-alkaline, high-K and shoshonitic fields in the K_2O *vs.* SiO_2 plot are after Peccerillo and Taylor (1976).

Fig. 4 Chondrite-normalized REE diagrams and primitive mantle-normalized spidergrams for the Jiurui and Edong "adakitic" plutonic rocks. Normalization values are from Sun and McDonough (1989).

Fig. 5 (A) Sr/Y *vs.* Y (after Defant et al., 2002) and (B) $(La/Yb)_N$ *vs.* Yb_N diagram (after Drummond and Defant, 1990) for the Jiurui and Edong "adakitic" plutonic rocks. A two-stage modeled Rayleigh fractionation from a calc-alkaline andesite melt is shown. Blue line indicates the first stage of magmatic fractionation (from andesite to dacite); green line implies the second stage of magmatic fractionation (from dacite to rhyolite). FC = fractional crystallization. Detailed discussion of the modeling is given in the text.

Fig. 6 Cathodoluminescence (CL) images for typical zircons from the Jiurui and Edong "adakitic" plutonic rocks. The small ellipses in the CL images

represent the spots of SIMS U-Pb and O isotope analyses; the large ellipses represent the spots of LA-MC-ICPMS Hf isotope analyses. The numbers in white, orange and yellow color fonts are the U-Pb dates (Ma), εHf(T) and $\delta^{18}O$ values, respectively. The white bars are 100 microns in length for scale. U-Pb dates are from X.H. Li et al. (2010).

Fig. 7 Histograms of zircon εHf(T) and $\delta^{18}O$ values and plot of zircon εHf(T) *vs.* $\delta^{18}O$ values for the ca. 145 Ma (A-C) and ca. 140 Ma (D-F) "adakitic" plutonic rocks from Jiurui and Edong mining districts.

Fig. 8 Initial $^{87}Sr/^{86}Sr$ (I_{Sr}) *vs.* εNd(T) plot for the Jiurui and Edong "adakitic" plutonic rocks. The fields of Sr-Nd isotopes for the LYRB Cretaceous basaltic rocks, the low-Mg adakitic rocks in Dabie Orogen and NE Yangtze Block and the Archean Kongling Group metamorphic rocks are after compilation of J.W. Li et al. (2009), Liu et al. (2010) and Ames et al. (1996).

Fig. 9 Rb *vs.* Sc plot for the Jiurui and Edong "adakitic" plutonic rocks. A two-stage modeled Rayleigh fractionation from a calc-alkaline andesite system is shown. Blue line indicates the first stage of magmatic fractionation (from andesite to dacite); green line implies the second stage of magmatic fractionation (from dacite to rhyolite). PM = partial melting; FC = fractional crystallization. Detailed discussion of the modeling is given in the text.

Fig. 10 K_2O *vs.* Na_2O plot for the Jiurui and Edong "adakitic" plutonic rocks. Slab-derived adakites are plotted (gray cross) for comparison (Data source: GEOROC at http://georoc.mpch-mainz.gwdg.de/georoc/).

Fig. 11 Correlations of (A) Sr vs. SiO_2, and (B) Sr vs. CaO for the Jiurui and Edong "adakitic" plutonic rocks, in comparison with those of the Dabie lower continental crust-derived high Sr/Y granitoids (HSG) and normal calc-alkaline granitoids (He et al., 2011)..

Fig. 12 Comparison of calculated magmatic $\delta^{18}O$ values between the LYRB adakitic

rocks and normal island arc volcanic rocks as well as other high Sr/Y rocks (slab-derived adakites, Archean orogenic TTGs, Archean post-orogenic sanukitoids, high-Mg andesites (HMAs) and the Setouchi lavas in SW Japan. Data are after compilation by Bindeman et al. (2005).

Fig. 13 K_2O/Na_2O-Sr-(Rb+Ba) triangle plot for comparison of the LYRB adakitic rocks to Archean post-orogenic sanukitoids (Krogstad et al., 1995; Smithies and Champion, 1999; Stevenson et al., 1999; Laurent et al., 2011), high Ba-Sr granites (Fowler and Henney, 1996; Qian et al., 2003; Ye et al., 2008; Choi et al., 2009), Setouchi lavas (Shimoda et al., 1998) and slab-derived adakites (data sources: GEOROC at http://georoc.mpch-mainz.gwdg.de/georoc/).

Fig. 14 Magmatic $\delta^{18}O$ vs. initial I_{Sr} plot for comparison of the LYRB adakitic rocks to Setouchi lavas (Shimoda et al., 1998; Bindeman et al. 2005) and Caledonian high Ba-Sr granites (Fowler and Henney, 1996). Distinct trends of source-contamination by sediment melt *vs.* crustal assimilation are after James (1981).

Fig. 15 Temporal and spatial distribution of the Yanshanian (Jurassic and Cretaceous) magmatism in eastern South China. Compilation of radiometric ages of the igneous rocks and their locations is presented in Appendix 4. Representative ages (Ma) are shown for well-dated magmatic rocks. The Yanshanian magmatism was initiated at 195-180 Ma around the Southern Jiangxi-Northeastern Guangdong Provinces (within the contour of 180 Ma magmatic front), and propagated with an outward-younging trend for the entire region (shown as contours of 160 Ma and 140 Ma magmatic front).

Fig. 16 A geodynamic modal accounting for the genesis of the Yanshanian magmatism in eastern South China during the Jurassic and early Cretaceous time. Detailed discussions are presented in the text.

A

Tarim Craton

North China Craton

Tibet

Songpan -Ganzi

Qinling - Dabie

TLF

Sulu

Yangtze Craton

JSF

Cathaysia

1000 km

B

115°

117°

119°

32°

30°

N

North China

Dabie

Tan-Lu Fault

Yangtze River

Yangtze

Fig. 1C

Fig. 1D

Ore-related adakites

Ore-barren adakites

30°10′ N

29°40′ N

C

Yangtze River

TLS

Daye

Linxiang

TSK

Yinzu

Yangxin

0 10 km

114°40′ E

115°20′ E

D

Yangtze River

Dengjiashan

Dongleiwan

Fengshan Ore Field

Wushan

Chengmenshan

Ruichang

0 5 km

29°50′ N

29°40′ N

115°30′ E

115°45′ E

Quaternary

Middle Triassic to Cretaceous strata

Devonian to Lower Triassic strata

Ordovician to Silurian strata

Cretaceous volcanic rocks

Granitoid intrusion

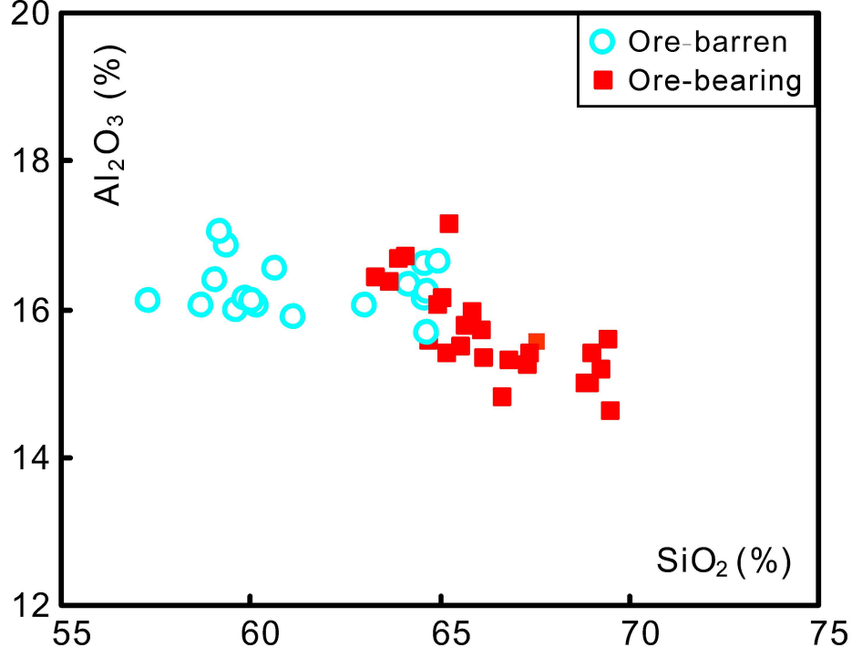
Ore-barren
Ore-bearing
Al_2O_3 (%)
SiO_2 (%)

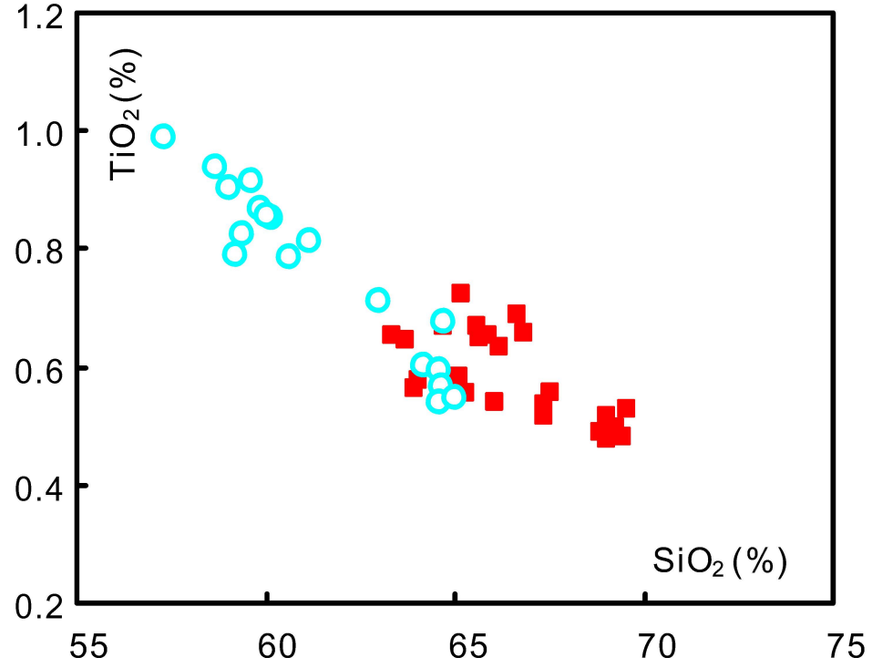
TiO_2 (%)
SiO_2 (%)

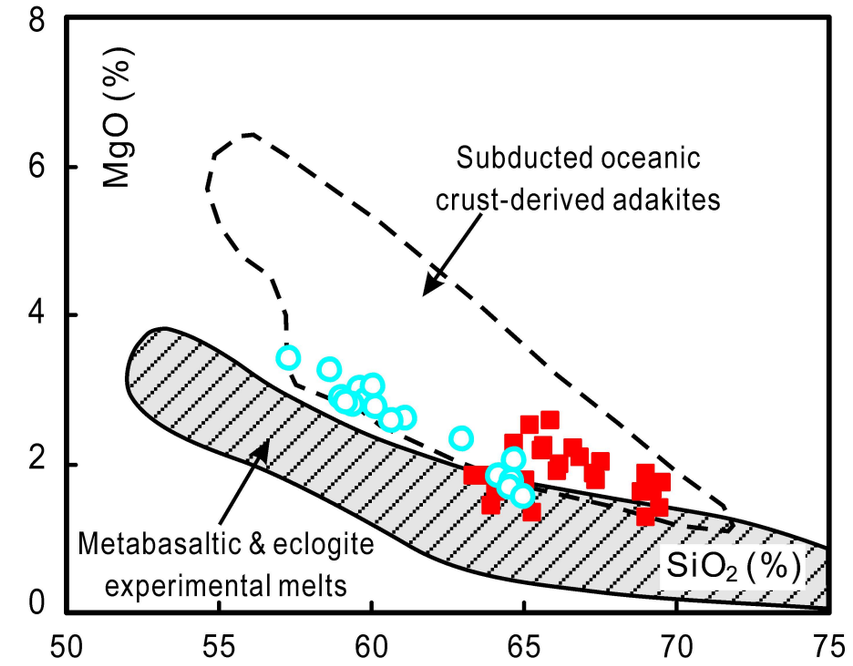
MgO (%)
Subducted oceanic
crust-derived adakites
Metabasaltic & eclogite
experimental melts
SiO_2 (%)

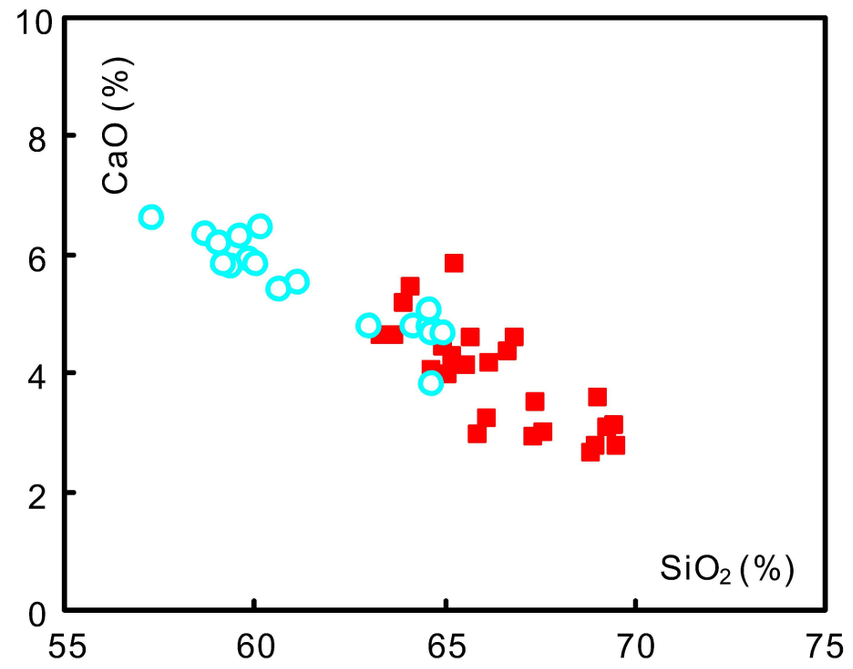
CaO (%)
SiO_2 (%)

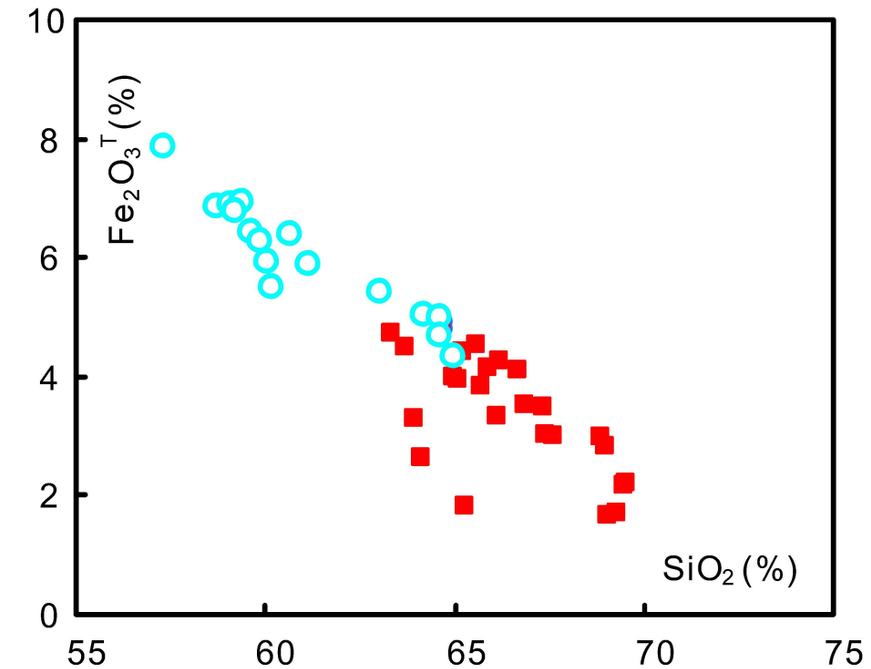
$Fe_2O_3^T$ (%)
SiO_2 (%)

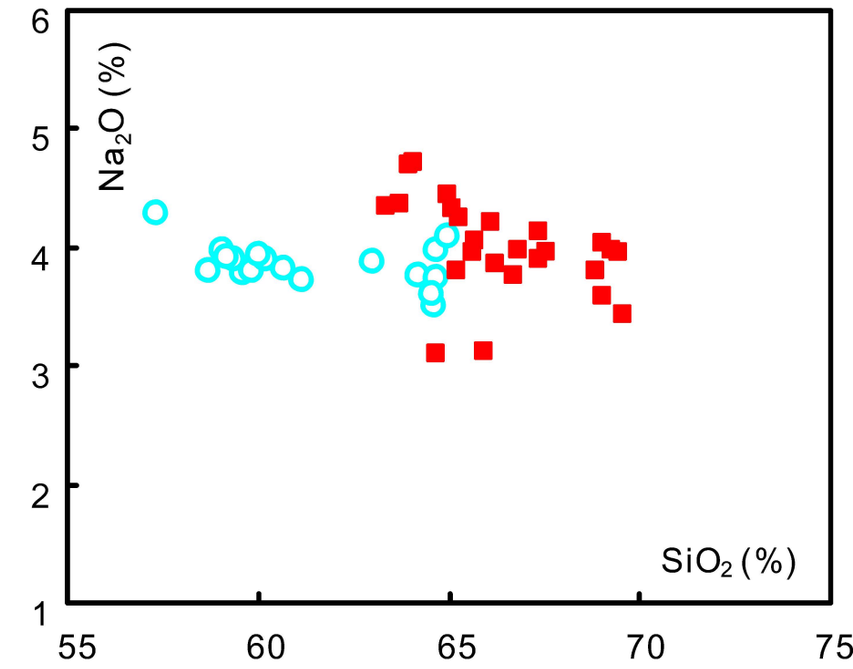
Na_2O (%)
SiO_2 (%)

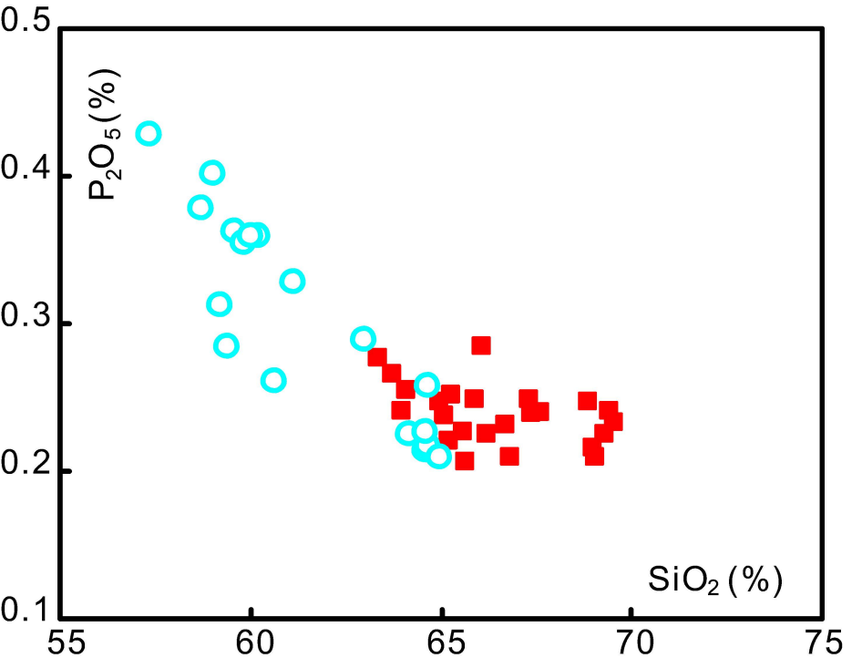
P_2O_5 (%)
SiO_2 (%)

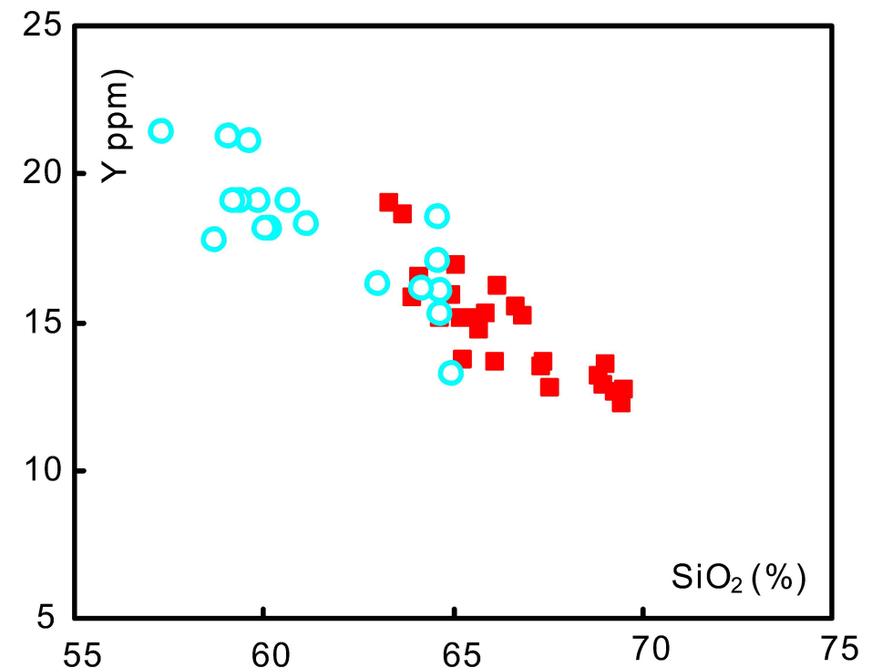
Y ppm)
SiO_2 (%)

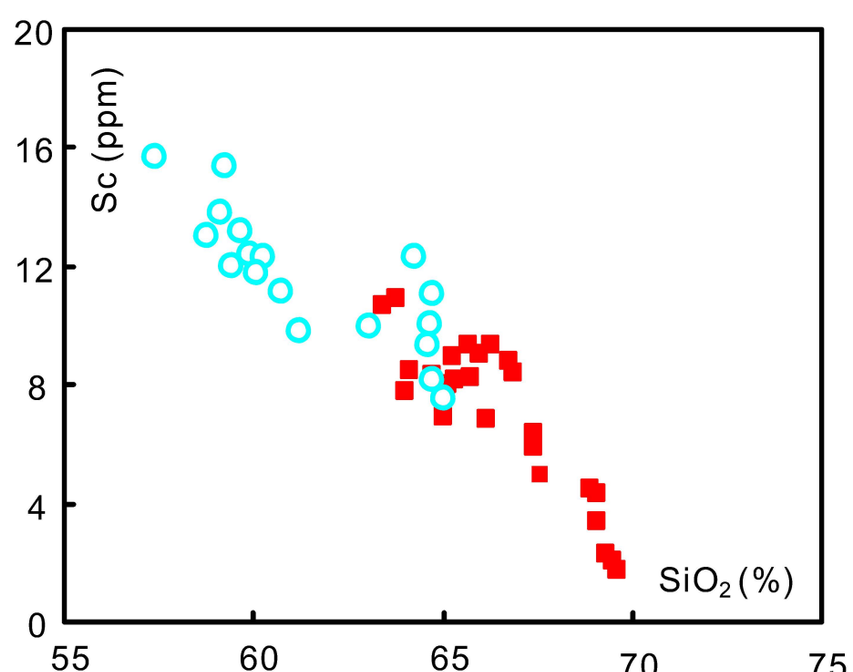
Sc (ppm)
SiO_2 (%)

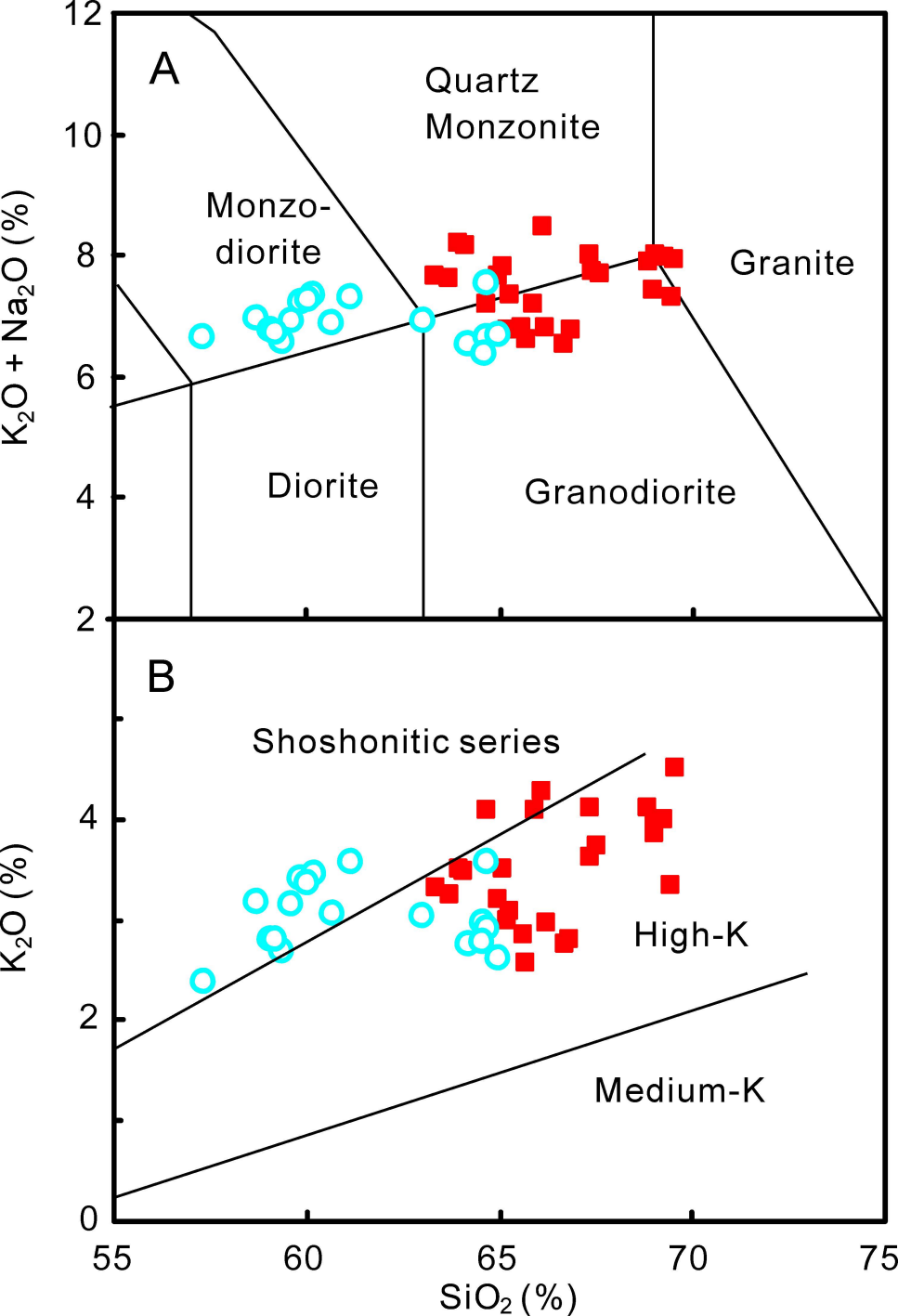
A
Quartz
Monzonite
Monzo-
diorite
Granite
Diorite
Granodiorite
$K_2O + Na_2O$ (%)
12
10
8
6
4
2
B
Shoshonitic series
High-K
Medium-K
K_2O (%)
4
2
0
55
60
65
70
75
SiO_2 (%)

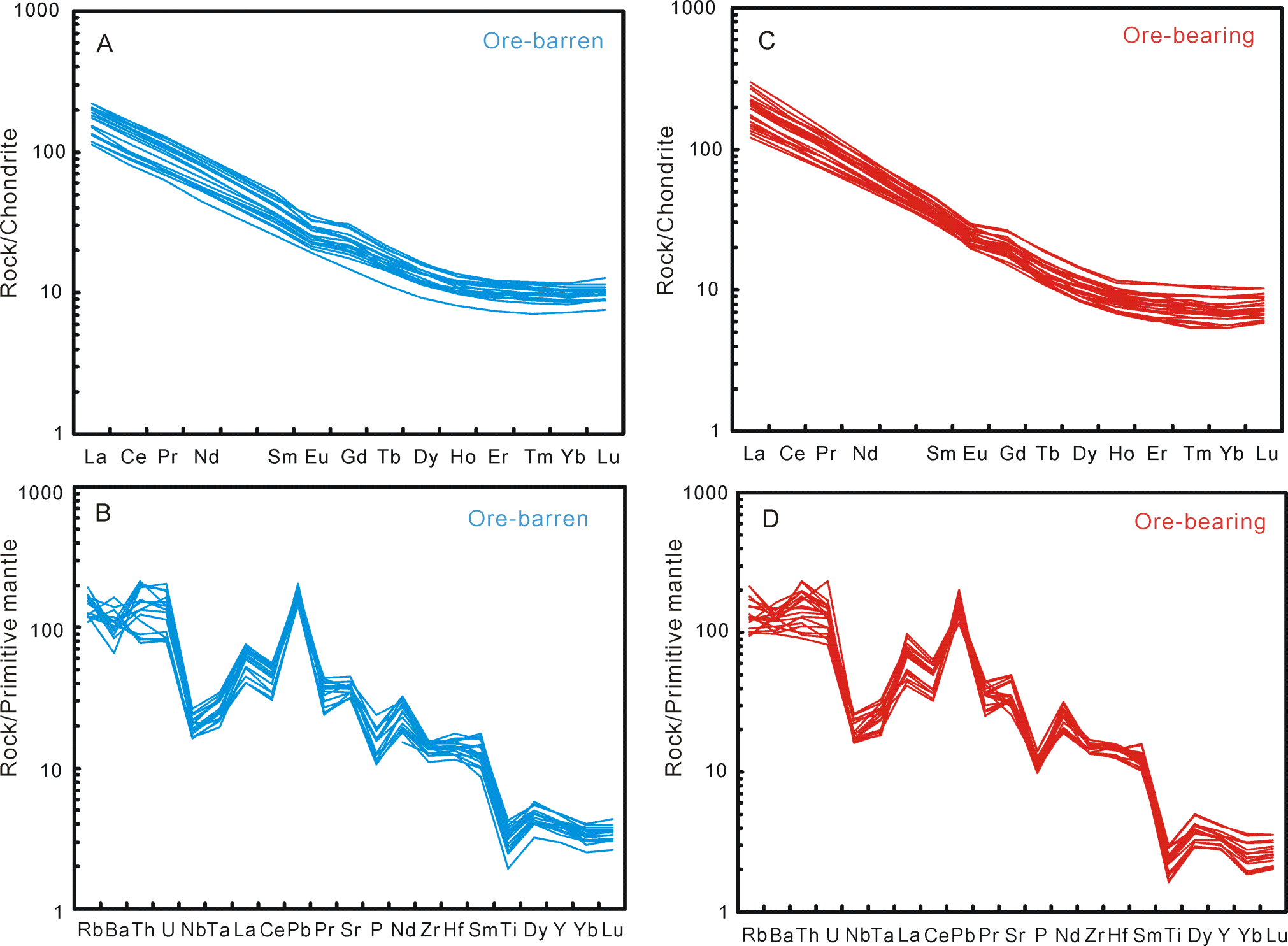
A
Ore-barren
Rock/Chondrite
1000
100
10
1
La Ce Pr Nd Sm Eu Gd Tb Dy Ho Er Tm Yb Lu
C
Ore-bearing
Rock/Chondrite
1000
100
10
1
La Ce Pr Nd Sm Eu Gd Tb Dy Ho Er Tm Yb Lu
B
Ore-barren
Rock/Primitive mantle
1000
100
10
1
Rb Ba Th U Nb Ta La Ce Pb Pr Sr P Nd Zr Hf Sm Ti Dy Y Yb Lu
D
Ore-bearing
Rock/Primitive mantle
1000
100
10
1
Rb Ba Th U Nb Ta La Ce Pb Pr Sr P Nd Zr Hf Sm Ti Dy Y Yb Lu

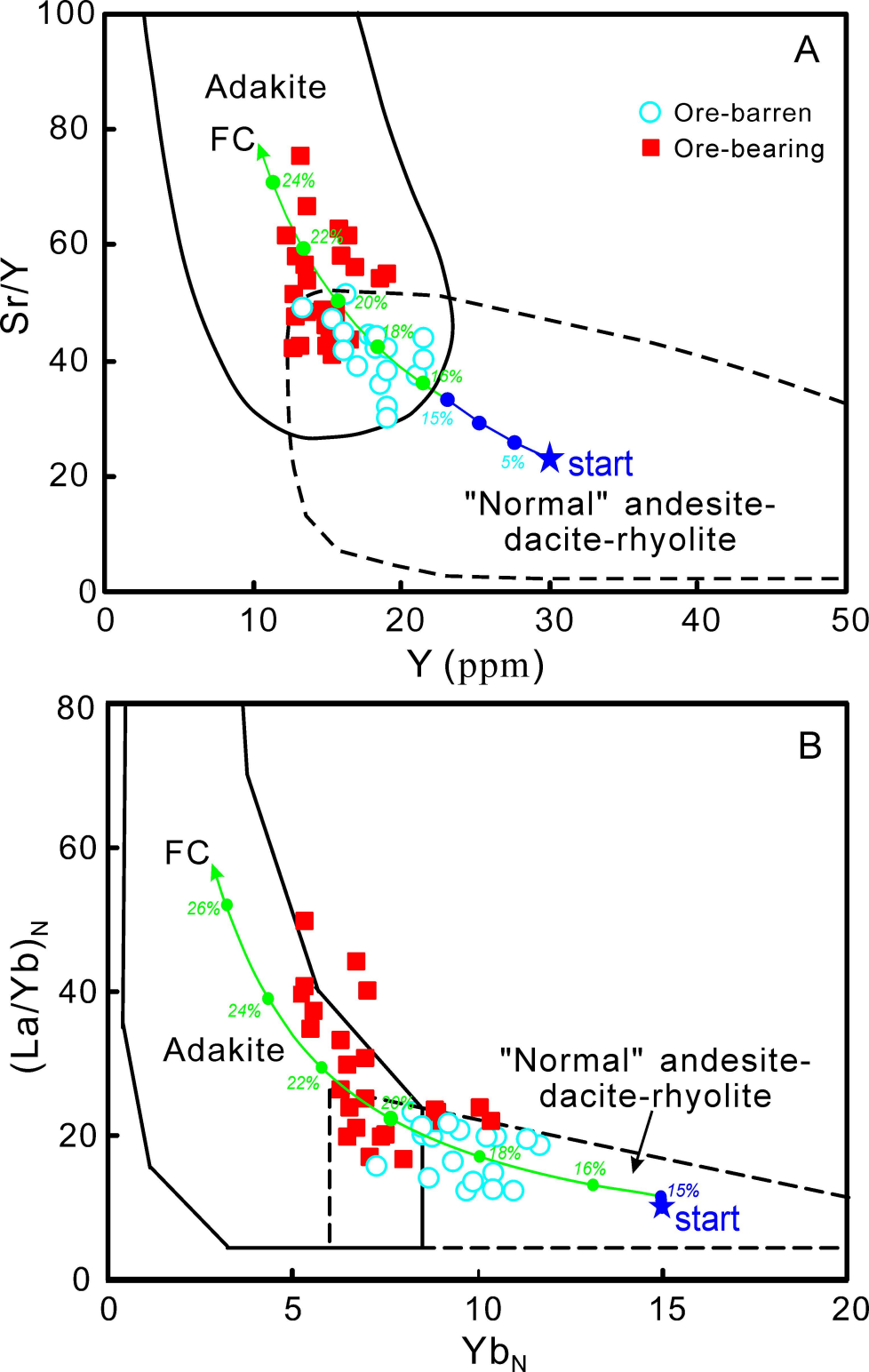
A
Adakite
FC
Ore-barren
Ore-bearing
24%
22%
20%
18%
16%
15%
5%
start
"Normal" andesite-
dacite-rhyolite
Sr/Y
Y (ppm)
0
20
40
60
80
100
0
10
20
30
40
50
B
FC
26%
24%
22%
20%
18%
16%
15%
start
Adakite
"Normal" andesite-
dacite-rhyolite
(La/Yb)N
YbN
0
20
40
60
80
0
5
10
15
20

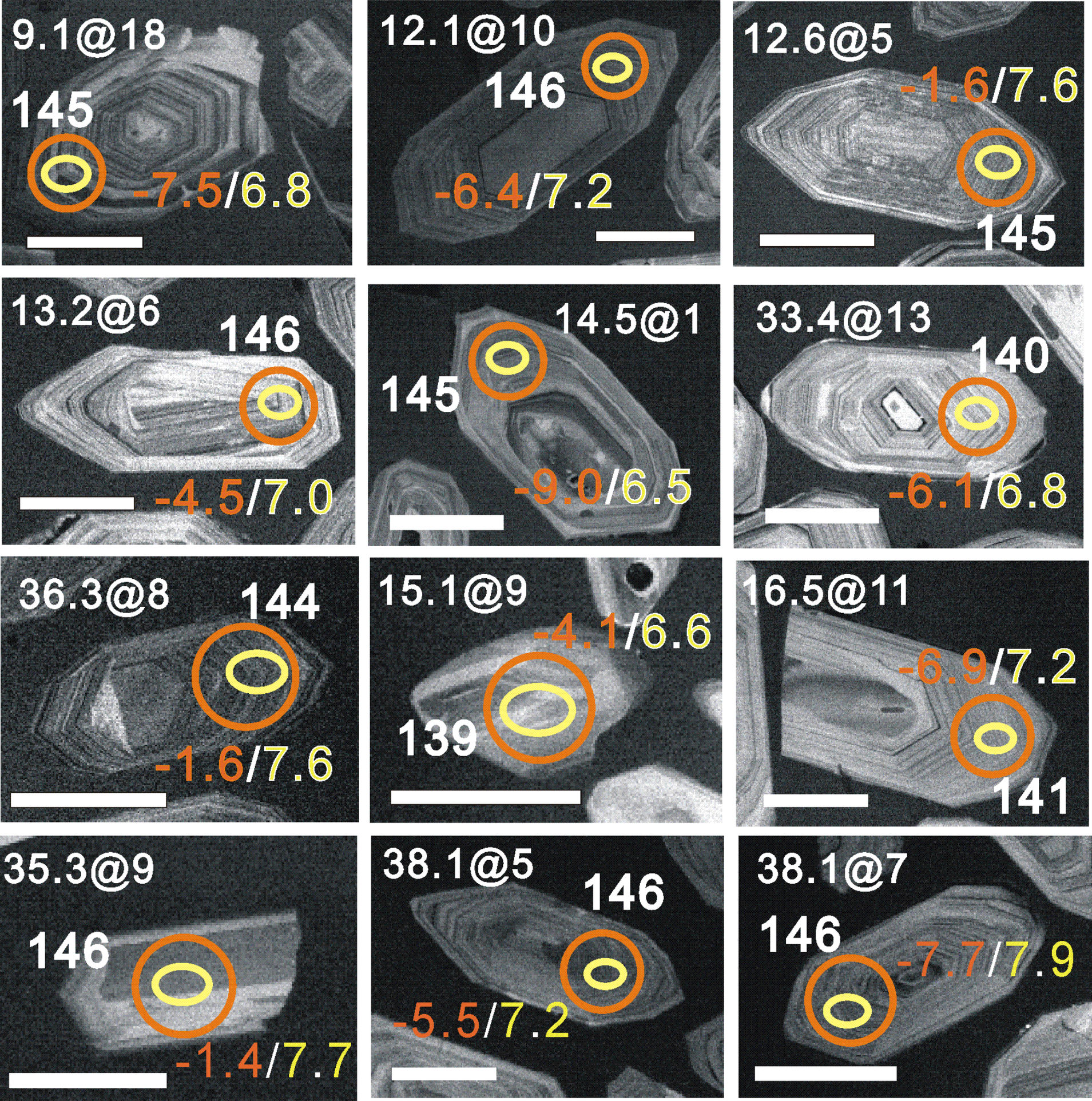
9.1@18
145
-7.5/6.8
12.1@10
146
-6.4/7.2
12.6@5
-1.6/7.6
145
13.2@6
146
-4.5/7.0
14.5@1
145
-9.0/6.5
33.4@13
140
-6.1/6.8
36.3@8
144
-1.6/7.6
15.1@9
-4.1/6.6
139
16.5@11
-6.9/7.2
141
35.3@9
146
-1.4/7.7
38.1@5
146
-5.5/7.2
38.1@7
146
-7.7/7.9

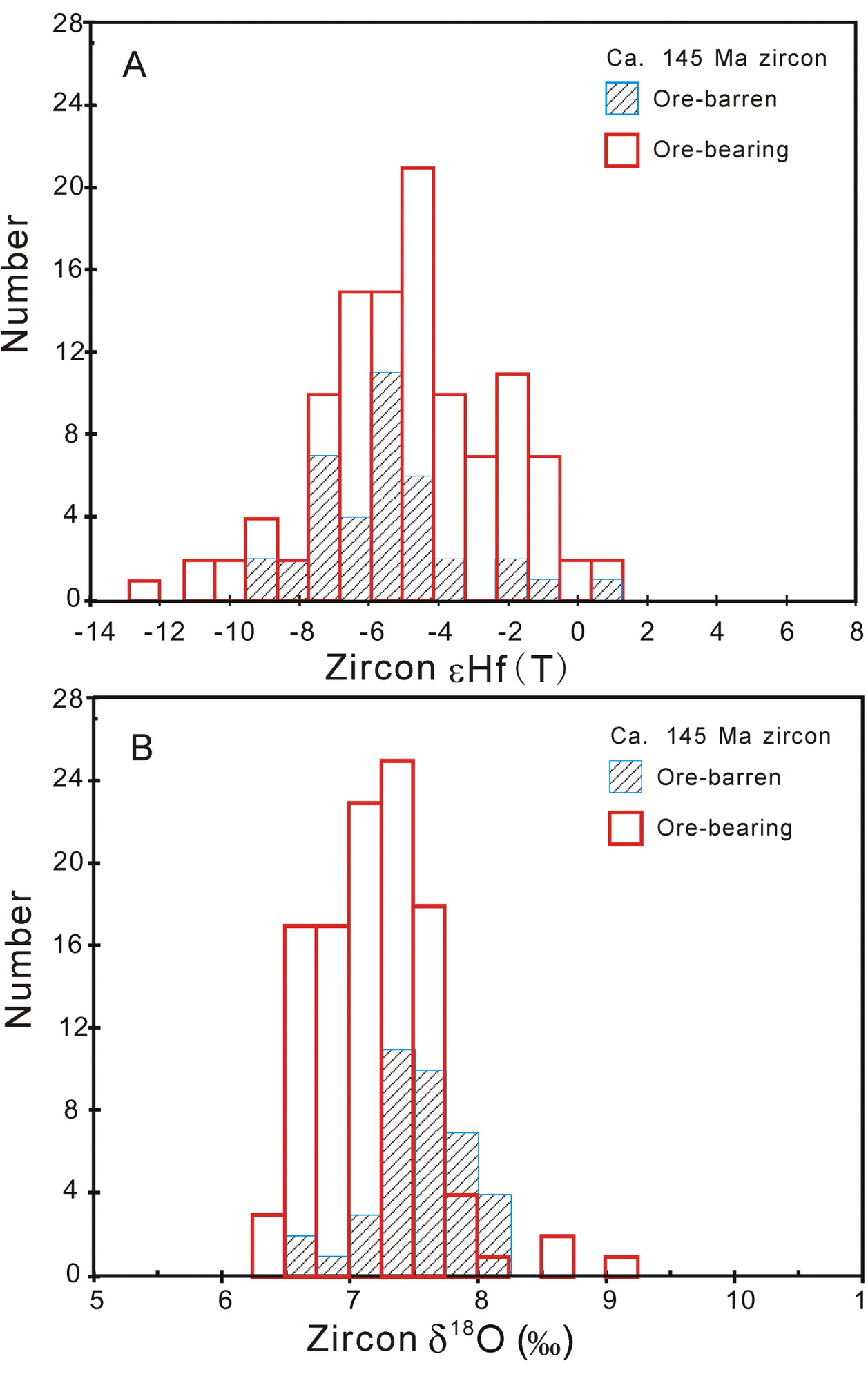
A
Ca. 145 Ma zircon
Ore-barren
Ore-bearing
Number
Zircon εHf(T)

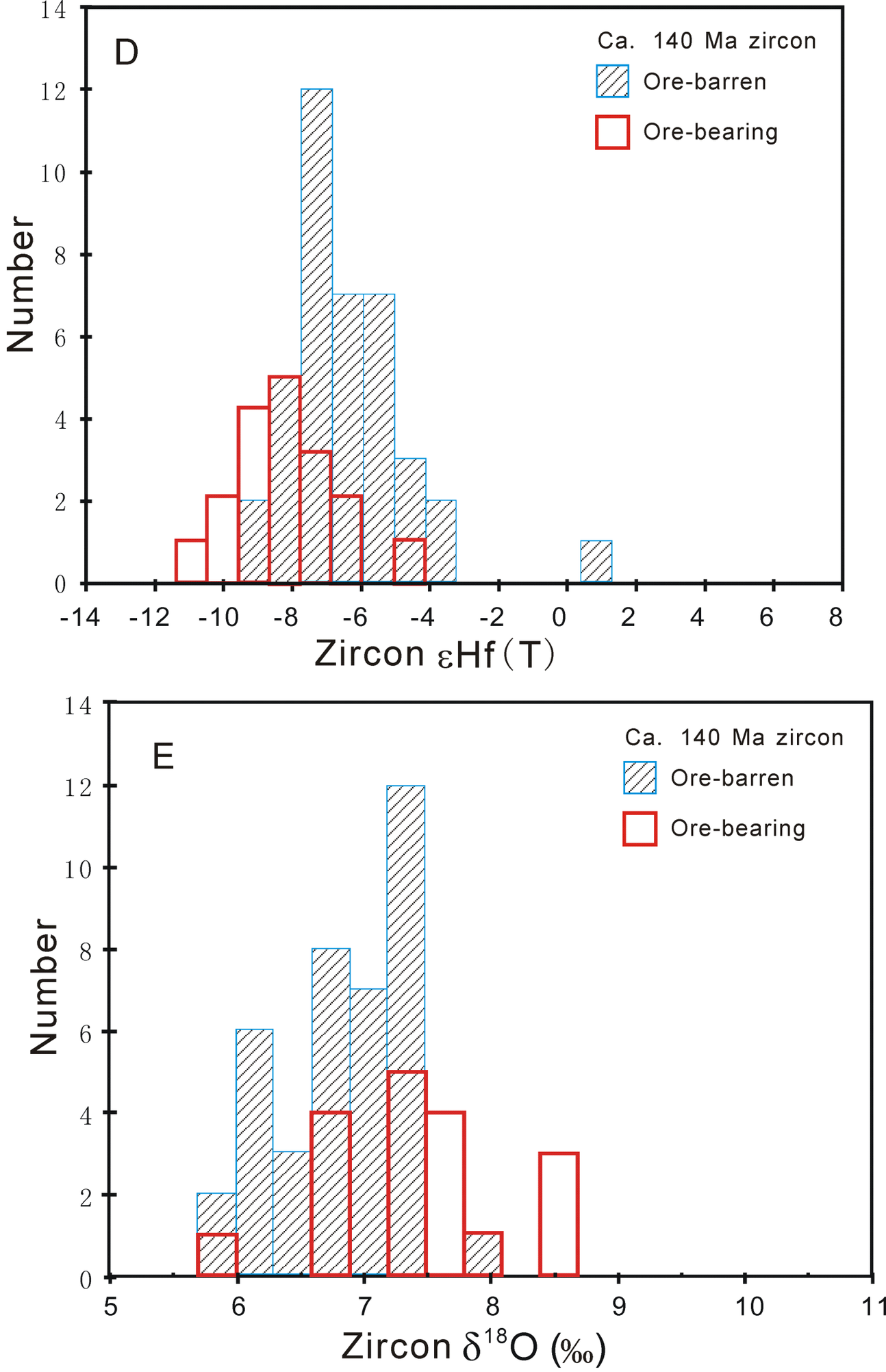
D
Ca. 140 Ma zircon
Ore-barren
Ore-bearing
Number
Zircon εHf(T)

B
Ca. 145 Ma zircon
Ore-barren
Ore-bearing
Number
Zircon δ18O (‰)

E
Ca. 140 Ma zircon
Ore-barren
Ore-bearing
Number
Zircon δ18O (‰)

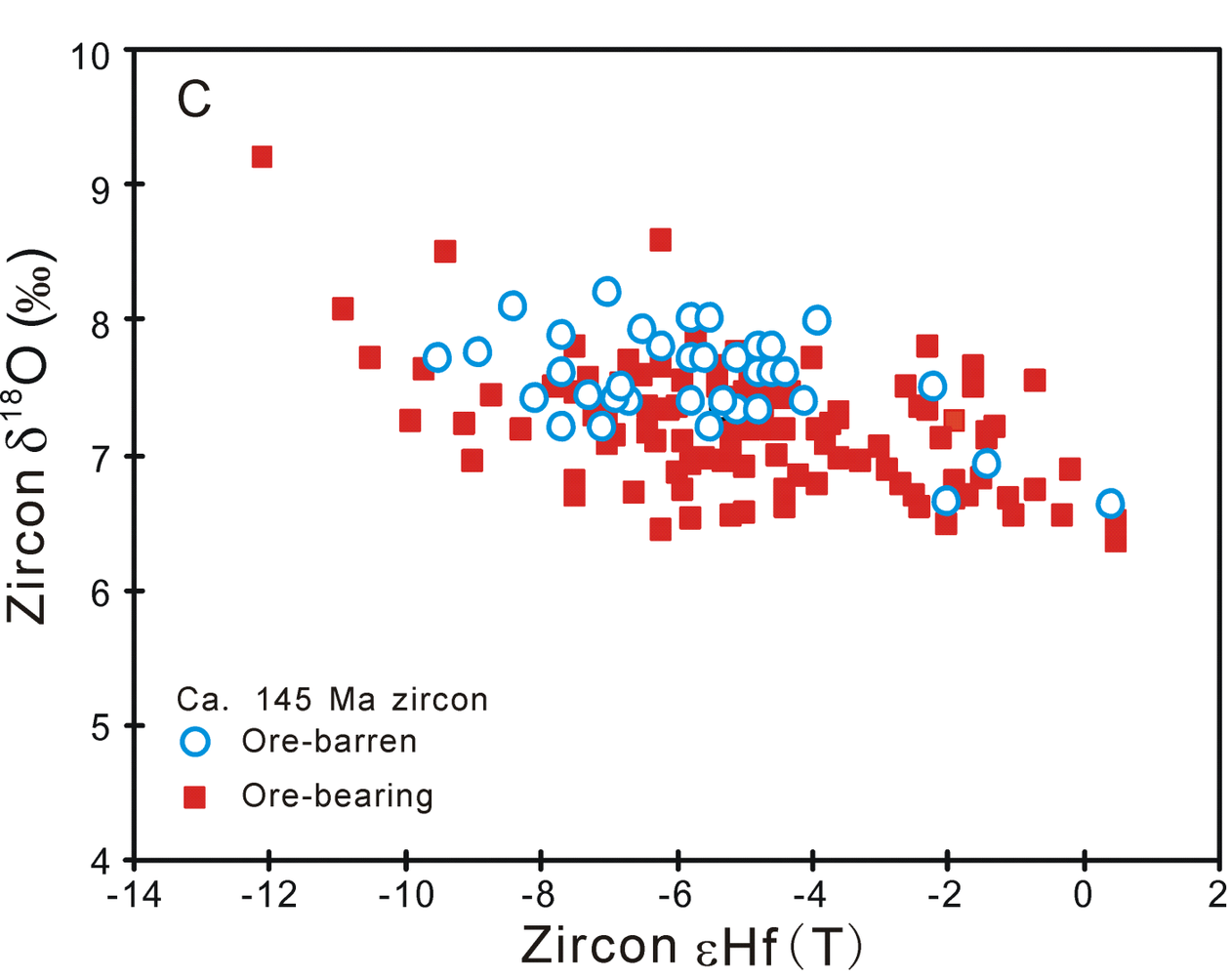
C
Ca. 145 Ma zircon
Ore-barren
Ore-bearing
Zircon δ18O (‰)
Zircon εHf(T)

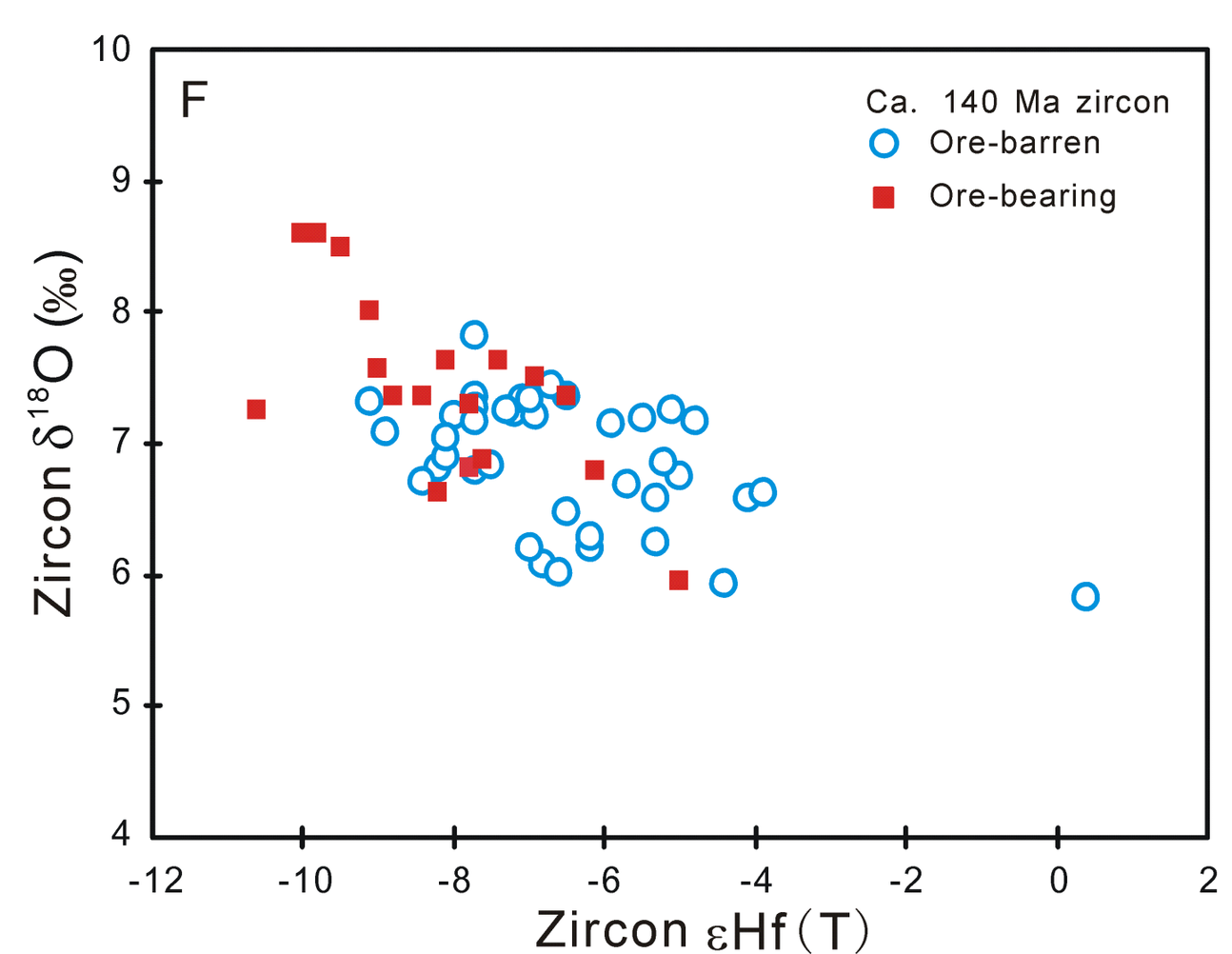
F
Ca. 140 Ma zircon
Ore-barren
Ore-bearing
Zircon δ18O (‰)
Zircon εHf(T)

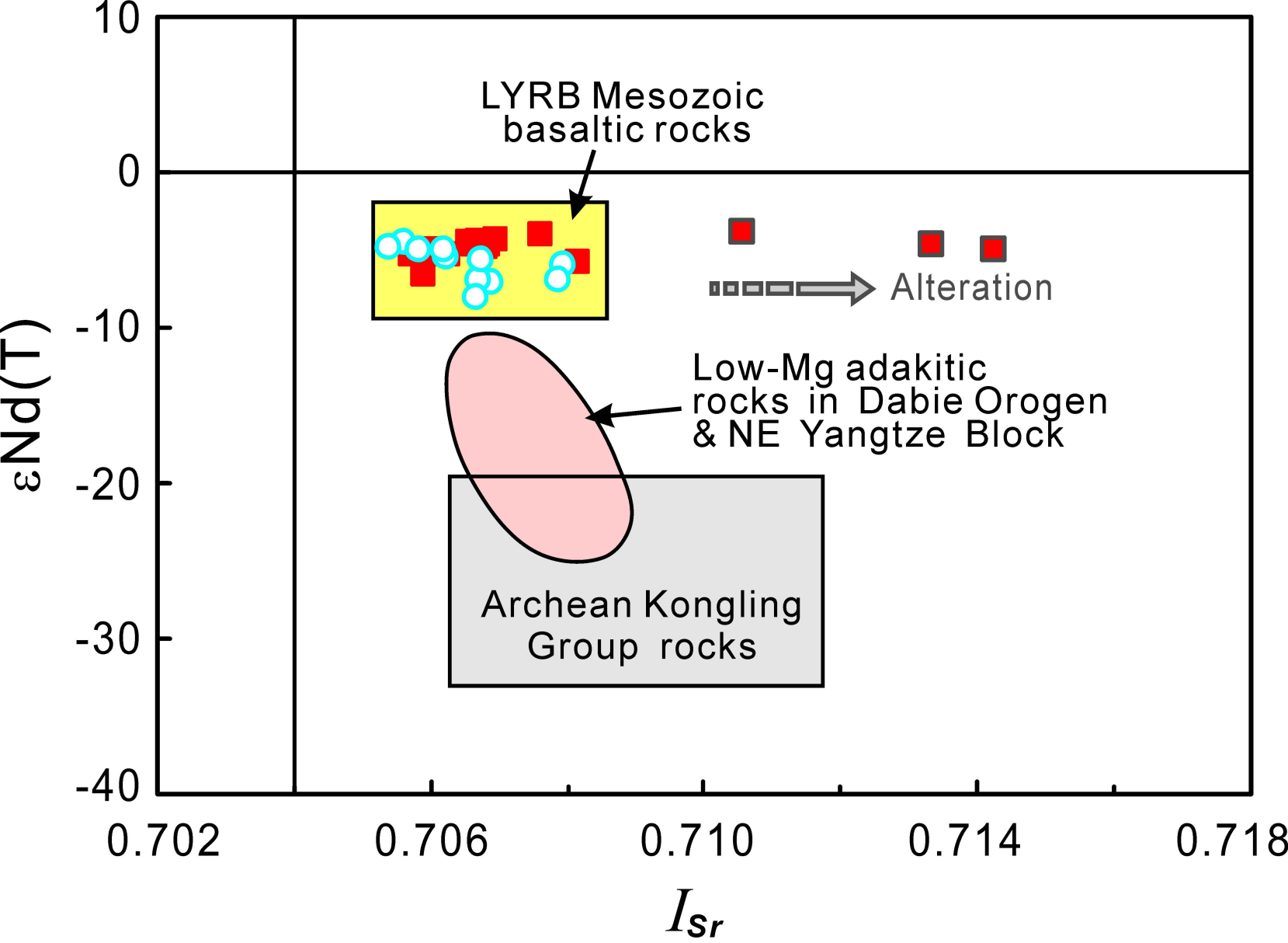

Archean Kongling gneiss (Ames et al. 1996),

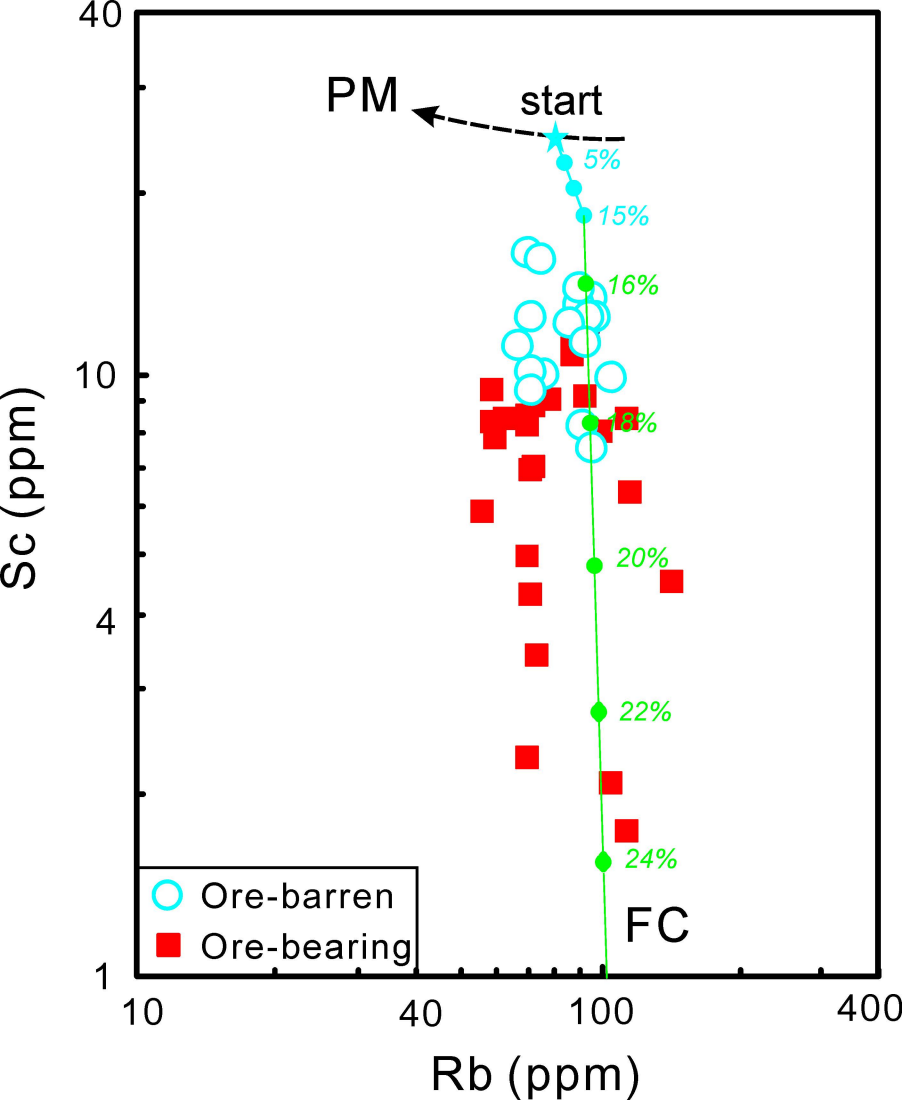
40
10
4
1
Sc (ppm)
10
40
100
400
Rb (ppm)
PM
start
5%
15%
16%
18%
20%
22%
24%
FC
Ore-barren
Ore-bearing

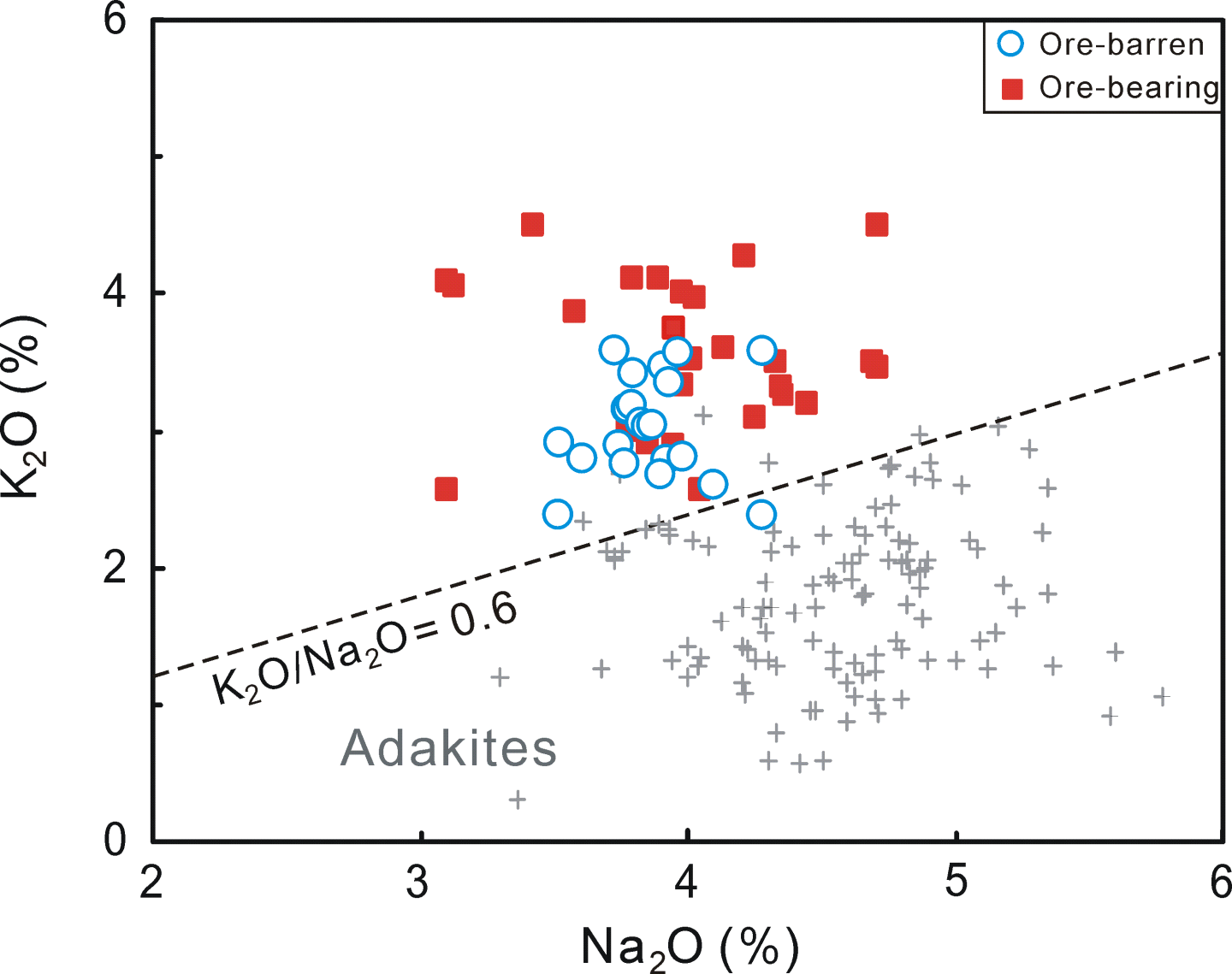
Ore-barren
Ore-bearing
$K_2O/Na_2O = 0.6$
Adakites
K_2O (%)
Na_2O (%)
0
2
4
6
2
3
4
5
6

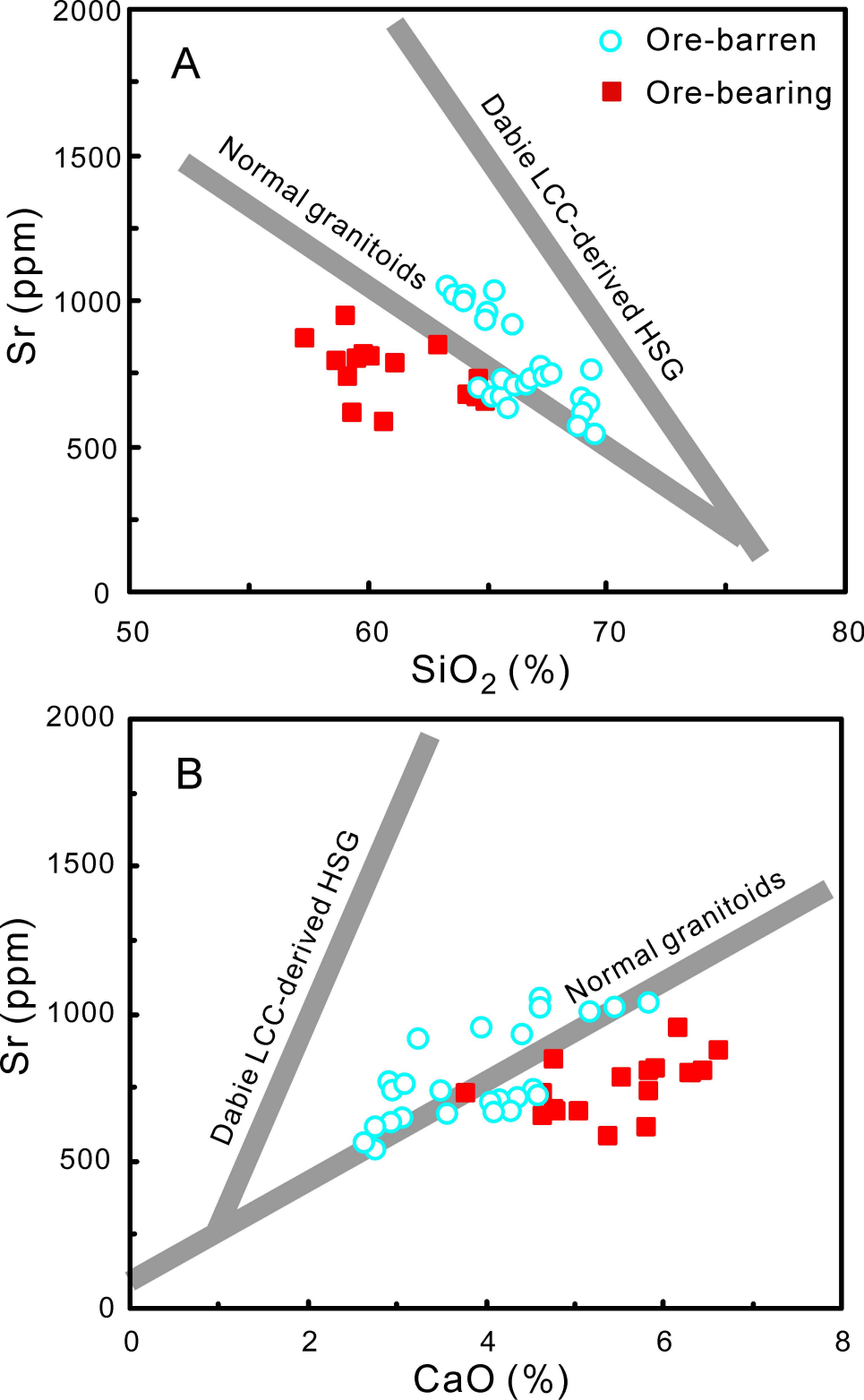
A
Ore-barren
Ore-bearing
Normal granitoids
Dabie LCC-derived HSG
Sr (ppm)
SiO2 (%)
2000
1500
1000
500
0
50
60
70
80
B
Dabie LCC-derived HSG
Normal granitoids
Sr (ppm)
CaO (%)
2000
1500
1000
500
0
0
2
4
6
8

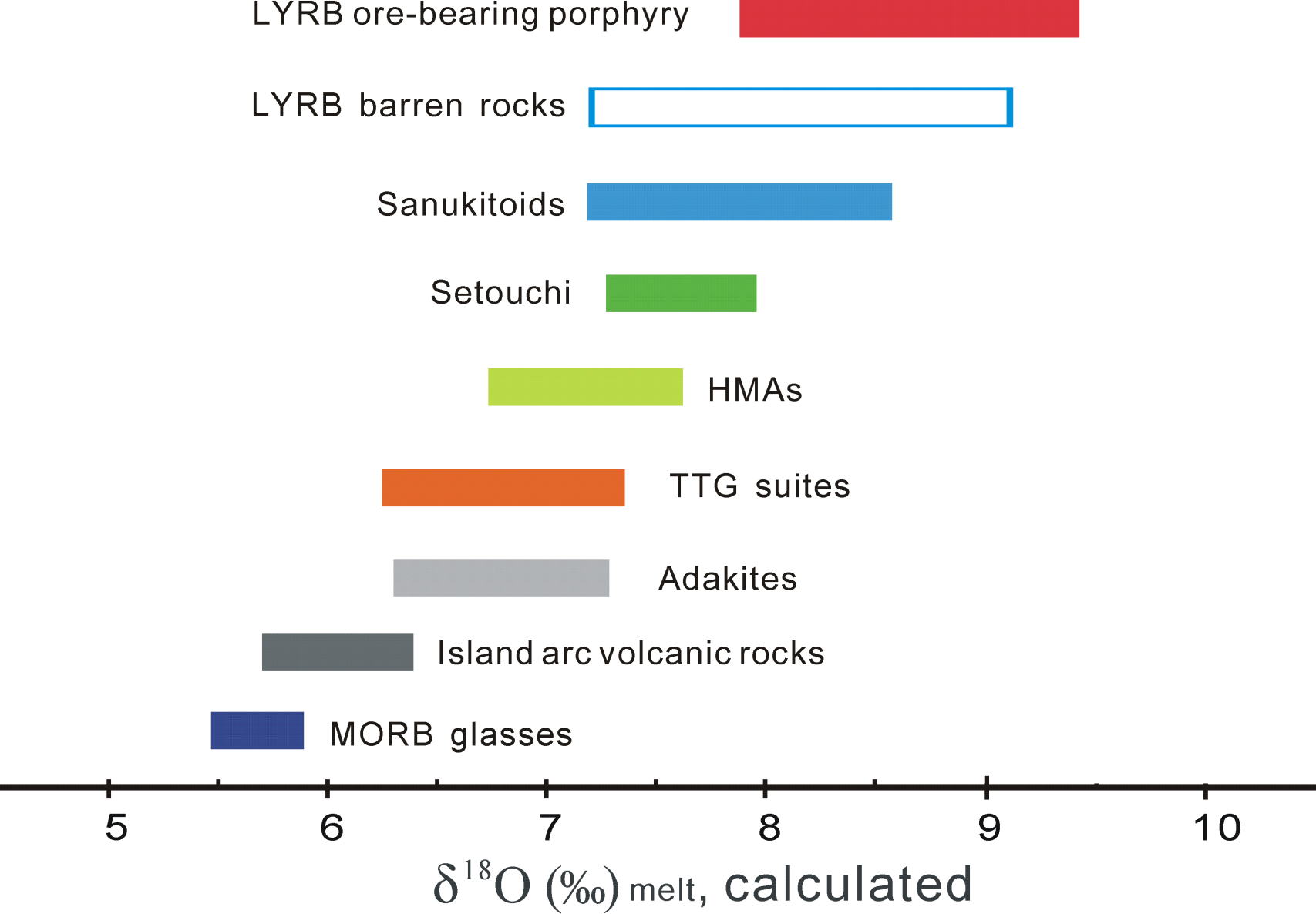
LYRB ore-bearing porphyry
LYRB barren rocks
Sanukitoids
Setouchi
HMAs
TTG suites
Adakites
Island arc volcanic rocks
MORB glasses
5
6
7
8
9
10
δ18O (‰) melt, calculated

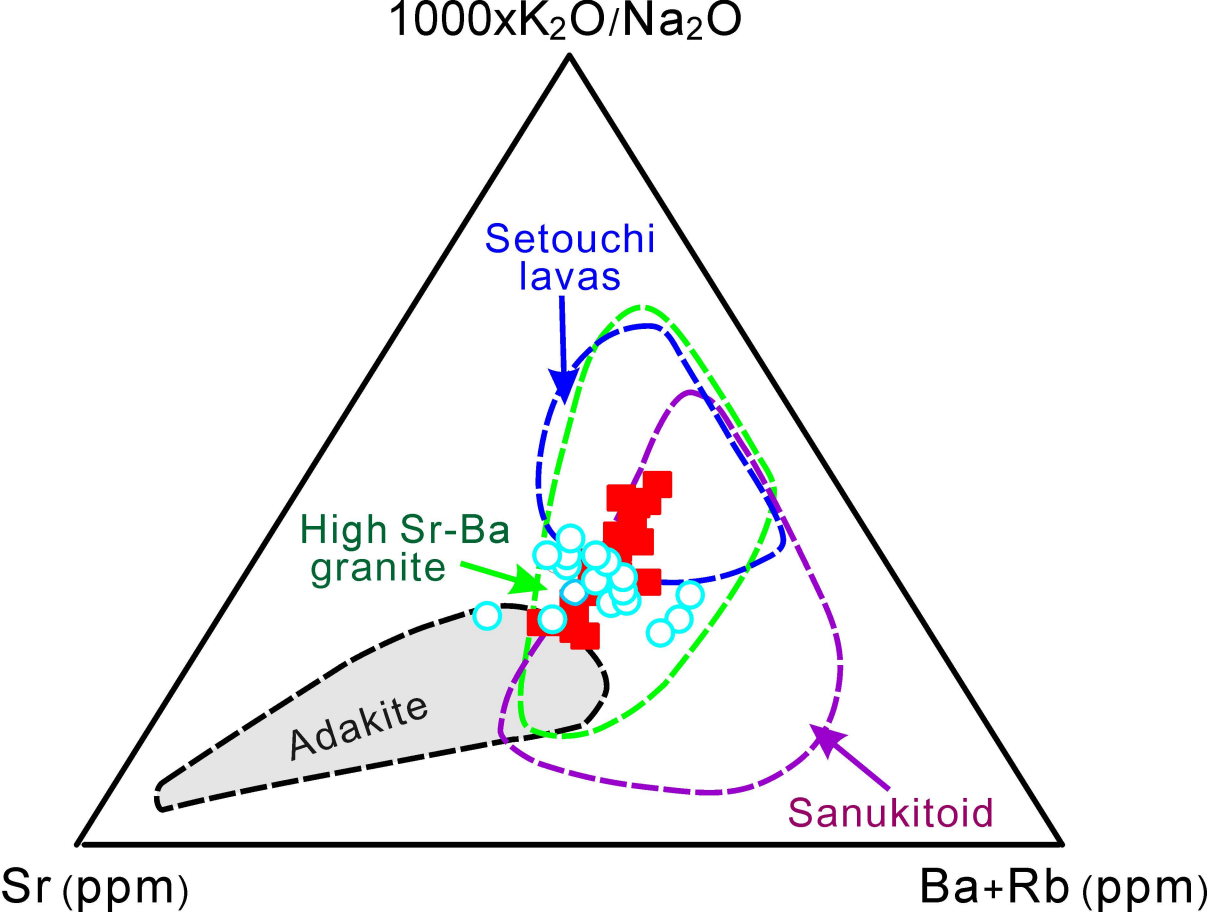
1000xK2O/Na2O
Setouchi lavas
High Sr-Ba granite
Adakite
Sanukitoid
Sr (ppm)
Ba+Rb (ppm)

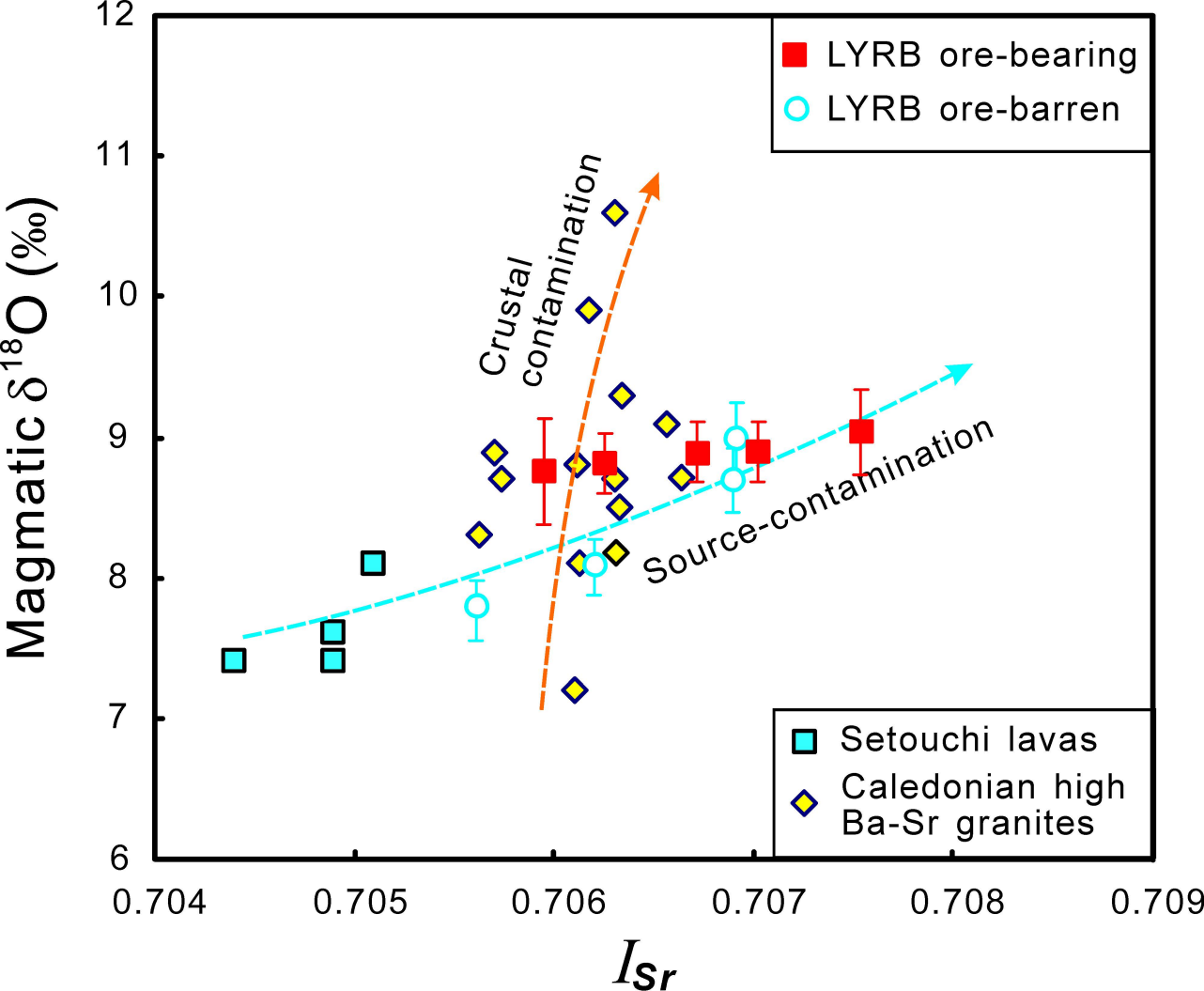
LYRB ore-bearing
LYRB ore-barren
Crustal contamination
Source-contamination
Setouchi lavas
Caledonian high Ba-Sr granites
Magmatic δ18O (‰)
Isr
12
11
10
9
8
7
6
0.704
0.705
0.706
0.707
0.708
0.709

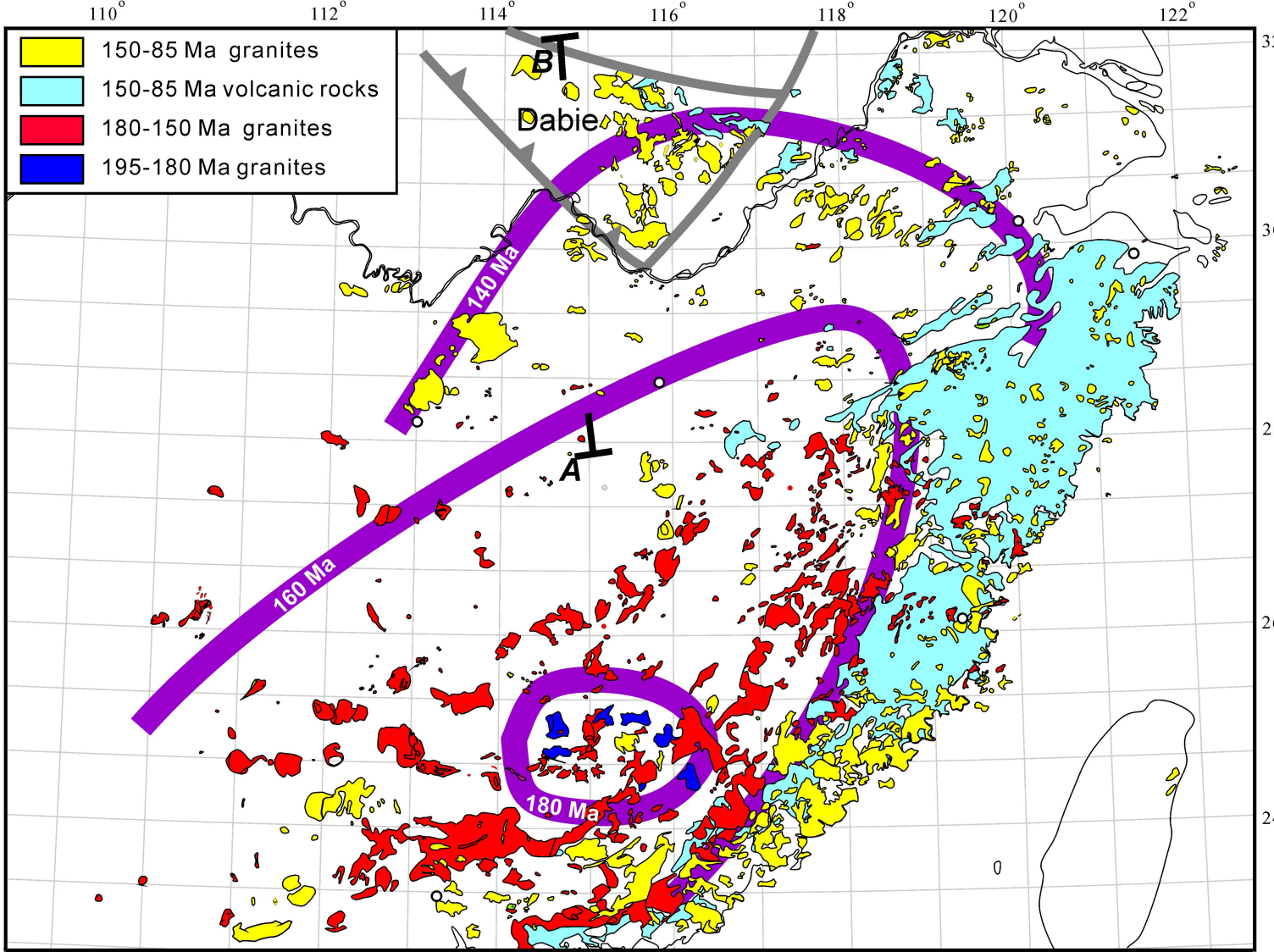
150-85 Ma granites
150-85 Ma volcanic rocks
180-150 Ma granites
195-180 Ma granites
B
Dabie
A
140 Ma
160 Ma
180 Ma
110°
112°
114°
116°
118°
120°
122°
32°
30°
28°
26°
24°

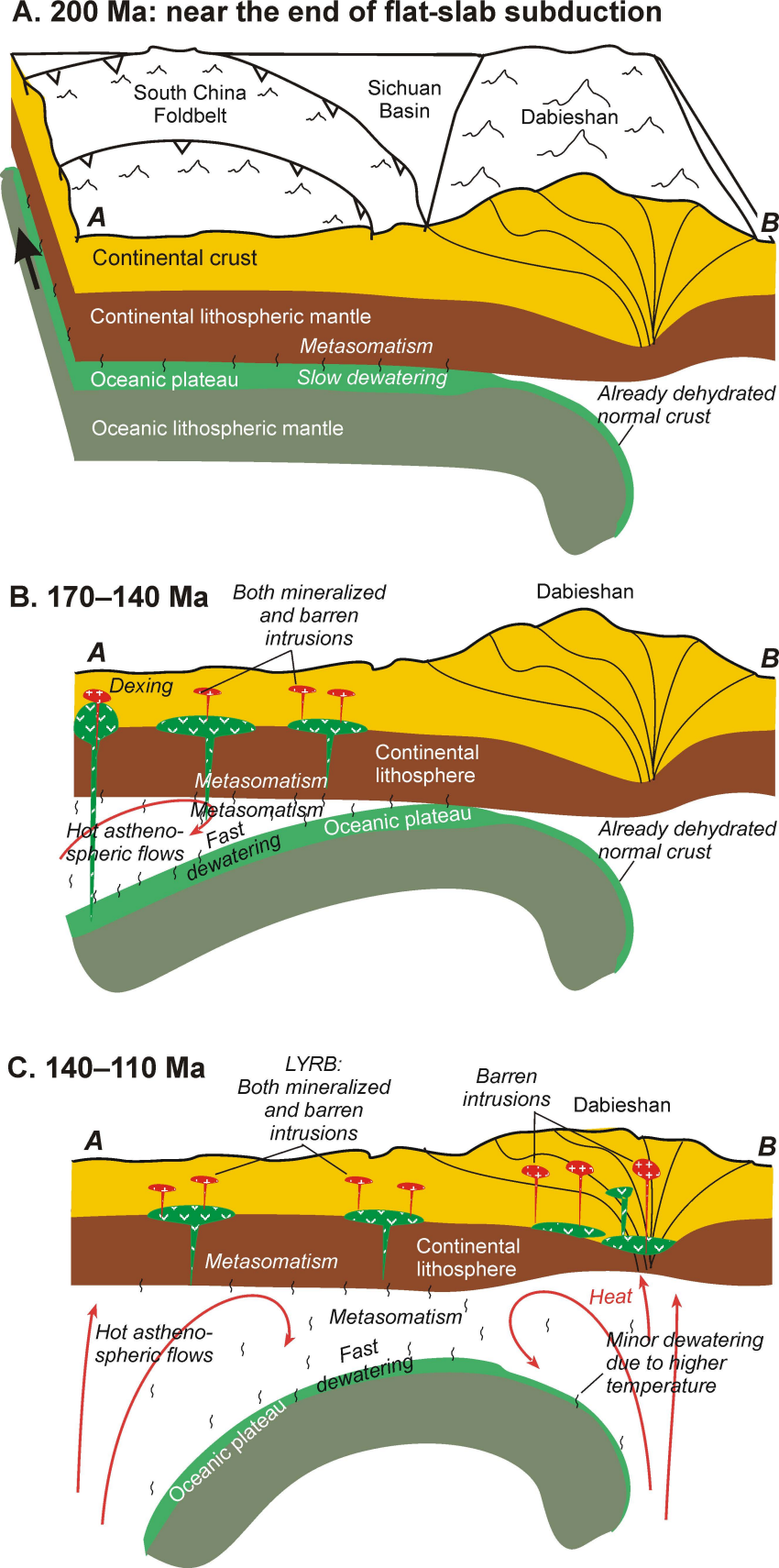
A. 200 Ma: near the end of flat-slab subduction
South China Foldbelt
Sichuan Basin
Dabieshan
A
B
Continental crust
Continental lithospheric mantle
Metasomatism
Oceanic plateau
Slow dewatering
Already dehydrated normal crust
Oceanic lithospheric mantle
B. 170–140 Ma
Both mineralized and barren intrusions
Dabieshan
A
B
Dexing
Continental lithosphere
Metasomatism
Metasomatism
Hot astheno-spheric flows
Fast dewatering
Oceanic plateau
Already dehydrated normal crust
C. 140–110 Ma
LYRB: Both mineralized and barren intrusions
Barren intrusions
Dabieshan
A
B
Metasomatism
Continental lithosphere
Heat
Metasomatism
Hot astheno-spheric flows
Fast dewatering
Minor dewatering due to higher temperature
Oceanic plateau